ON COSMOLOGICAL SUPERNOVA OBSERVATIONS AND ALTERNATIVE GRAVITY THEORIES

by

Mehmet Akif Feyizoğlu

B.S., Physics, Boğaziçi University, 2015

Submitted to the Institute for Graduate Studies in
Science and Engineering in partial fulfillment of
the requirements for the degree of
Master of Science

Graduate Program in Physics

Boğaziçi University

2019

ACKNOWLEDGEMENTS

I would first like to thank my supervisor, Prof. İbrahim Semiz, and cosupervisor, Assist. Prof. Ali Kazım Çamlıbel. Their doors were always open whenever I ran into a trouble spot or had a question about my research or writing. They consistently allowed this thesis to be my own work, but steered me in the right direction whenever they thought I needed it.

Finally, I must express my very profound gratitude to my parents for providing me with unfailing support and continuous encouragement throughout my years of study and through the process of researching and writing this thesis. This accomplishment would not have been possible without them. Thank you.

ABSTRACT

ON COSMOLOGICAL SUPERNOVA OBSERVATIONS AND ALTERNATIVE GRAVITY THEORIES

This thesis is about getting the most information from the cosmological supernova data about the expansion history of the homogeneous and isotropic universe, with the least possible set of assumptions. To this end, we fit various functions to the luminosity distance $d_L(z)$ and try to reconstruct the scale factor $a(t)$, through the best of those functions, without an assumption of gravity models; hence making this analysis *model-independent*. We find that with the SNe Ia data we can show the current acceleration and past deceleration of the universe. However, to get even better results, we add gamma ray burst data to the dataset at the cost of slightly compromising the model-independent nature of the analysis. With this expanded data set, we can determine the redshift of transition from deceleration in the past to current acceleration as $z_t \approx 0.55 \pm 0.08$ for a flat universe (larger for positive spatial curvature, and smaller for negative). In this work, we see that the choice of parametrization heavily affects the results of the analysis.

After the assumption of Einstein's General Relativity, we see that, as in previous work, there is a special redshift value at which the curvature of the universe has no effect on its energy density. Using this redshift value, we manage to put an upper limit on matter density, hence a lower limit on the density of dark energy. If Starobinsky's gravity model is assumed, we find that from the positive α values (parameter of Starobinsky model) we cannot get anything useful however from a certain negative value we get energy density curve very close to the matter-only curve. Hence, we can find a simple modified-gravity cosmology with no dark energy, but with about twice as much dark matter as the concordance model.

ÖZET

KOZMOLOJİK SÜPERNOVA GÖZLEMLERİ VE ALTERNATİF ÇEKİM TEORİLERİ ÜZERİNE

Bu tez, mümkün olan en az varsayımla, homojen ve izotropik evrenin genişleme tarihi hakkında kozmolojik süpernova verilerinden en fazla bilgiyi elde etmekle ilgilidir. Bu amaçla, parlaklık mesafesi $d_L(z)$'ye çeşitli fonksiyonlar uyduruyoruz ve ölçek faktörü $a(t)$'yi bu fonksiyonların en iyilerini kullanarak ve genelçekim modelleri varsayımı olmadan inşa ediyoruz, yani modelden bağımsız bir analiz yapıyoruz. Tip Ia süpernova verileriyle, evrenin mevcut ivmelenmesini ve geçmiş yavaşlamasını gösterebiliyoruz. Ayrıca, daha iyi sonuçlar elde etmek için, analizin modelden bağımsız olma özelliğinden hafifçe ödün verme pahasına, veri setine gama ışını patlamaları verilerini de ekliyoruz. Bu genişletilmiş veri seti ile, düz bir evren için, geçmişteki yavaşlamadan mevcut hızlanmaya geçiş kızılakaymasını, $z_t \approx 0.55 \pm 0.08$, olarak belirleyebiliyoruz (pozitif eğrilik için daha büyük, negatif için daha küçük). Bu çalışmada, parametre seçiminin analizin sonuçlarını önemli ölçüde etkilediğini görüyoruz.

Einstein'ın Genel Göreliliği varsayımını yaparsak, ilgili önceki çalışmada olduğu gibi, evrenin eğriliğinin enerji yoğunluğu üzerinde hiçbir etkisinin olmadığı özel bir kızılakayma değeri olduğunu görüyoruz. Bu kızılakayma değerini kullanarak madde yoğunluğuna bir üst sınır, dolayısıyla karanlık enerjinin yoğunluğuna bir alt sınır getirebiliyoruz. Eğer Starobinsky'nin genelçekim modeli varsayılırsa, pozitif α için (Starobinsky modelinin parametresi) faydalı bir sonuç elde edilemediğini, belli bir negatif değer için ise, gerçekteki enerji yoğunluğu eğrisine çok yakın çizdirilebilen bir madde-baskın yoğunluk eğrisi olduğunu buluyoruz. Yani, karanlık enerjinin olmadığı, ama genel kabul gören modele göre iki misli karanlık madde içeren bir modifiye-genelçekim kozmolojisi bulabiliyoruz.

TABLE OF CONTENTS

LIST OF FIGURES

LIST OF TABLES

LIST OF SYMBOLS

$a(t), a(z)$	Scale factor of the universe
c	Speed of light
d_L	Luminosity distance
d_m	Uncalibrated luminosity distance
D	Photon count distance
G	Gravitational constant
H	Hubble parameter
I	Intensity
k	Curvature parameter
K	Kinetic energy
L	Luminosity
p	Pressure
$\tilde{P}$	Padé approximant
R	Ricci scalar
q	Deceleration parameter
V	Volume
z	Redshift
α	$f(R)$ parameter
κ	Curvature function
λ	Wavelength
Λ	Cosmological constant
ρ	Energy density
Ω	Energy density fraction

LIST OF ACRONYMS/ABBREVIATIONS

CDM	Cold Dark Matter
CMB	Cosmic Microwave Background
DE	Dark Energy
DM	Dark Matter
EoS	Equation of State
FRW	Friedman-Robertson-Walker
GR	General Relativity
GRB	Gamma Ray Burst
MD	Matter Dominated
SN	Supernova
SN Ia	Supernova type Ia

1. INTRODUCTION

Observational cosmology is the study of the origin, the structure and the evolution of the universe through analysis of observations. The analysis methods include not only analytic techniques, but also various data mining and numerical methods. In this thesis; firstly we will be focusing on the expansion history of the universe with minimal assumptions, and secondly we will calculate the energy density history of the universe for two assumed gravity models.

The research about the expansion of the universe can be traced back to the observations of Edwin Hubble [1]. The method of inquiry has not changed much since then; measure the redshift of a distant object for which you can evaluate a distance indicator separately. These objects then become test particles acting as flags on the observable universe. They will be used as data points to get the scale factor of the universe, which will give the expansion of space as a function of time in the framework of the isotropic and homogeneous cosmology. Here the spatial curvature of the universe will be the only free parameter, which can be constrained using other observations or theories. Generally, this kind of analysis is called cosmography or the model-independent approach.

Object of known luminosity (radiative power) are called standard candles. For these, one can define luminosity distance d_L as

$$d_L^2(z) \equiv \frac{L}{4\pi I}, \tag{1.1}$$

the distance an object of known luminosity (radiative power) L would have if it creates an intensity I in our telescopes and *if the universe was assumed to be flat and static* (i.e Minkowski space).

The most useful standard candles for cosmology are the type Ia supernova (SNe Ia) events; their observation data are made up of measurements of their redshifts z

and their distance moduli μ. The luminosity distance can be calculated in terms of the distance moduli by

$$d_L(z) = 3.26 \times 10^{0.2\mu+1} \text{ ly}. \tag{1.2}$$

The metric, which follows from the assumptions of homogeneity and isotropy, is called the Friedman-Robertson-Walker (FRW) metric and can be represented by the line element

$$ds^2 = -c^2dt^2 + a^2(t)\left[\frac{dr^2}{1-kr^2} + r^2\left(d\theta^2 + \sin^2\theta d\phi^2\right)\right]. \tag{1.3}$$

1.1. Redshift, scale factor and luminosity distance

To see the link between scale factor and redshift consider the light during its travel from the source to us. The light travels along the null geodesics, with $ds = 0$. The null geodesic has θ and ϕ constant. Hence, along the light's path,

$$c^2dt^2 = a^2(t)\frac{dr^2}{1-kr^2} \tag{1.4}$$

and

$$\frac{cdt}{a(t)} = \pm\frac{dr}{\sqrt{1-kr^2}} \tag{1.5}$$

Note that; the left hand side is a function only of t, and the right hand side is independent of t. Integrating this we get,

$$c\int_{t_1}^{t_0}\frac{dt}{a(t)} = -\int_{r_1}^{0}\frac{dr}{\sqrt{1-kr^2}} = f_k(r_1) \tag{1.6}$$

for a wave crest of light traveling from r_1 to the $r = 0$ in time interval of t_1 to t_0. Now imagine that next wave crest of light is emitted at a time $t = t_1 + dt_1$ at r_1, and is observed at $t = t_0 + dt_0$ at $r = 0$. For the second wave crest we get,

$$c\int_{t_1+dt_1}^{t_0+dt_0}\frac{dt}{a(t)} = -\int_{r_1}^{0}\frac{dr}{\sqrt{1-kr^2}} = f_k(r_1) \tag{1.7}$$

comparing the equation for the first and the second wave crest leads to;

$$\int_{t_1}^{t_0}\frac{dt}{a(t)} = \int_{t_1+dt_1}^{t_0+dt_0}\frac{dt}{a(t)} \tag{1.8}$$

and this is simply,

$$\frac{dt_0}{a(t_0)} = \frac{dt_1}{a(t_1)} \tag{1.9}$$

So we find that the redshift of light from a source is related to the expansion factor at the time it was emitted by the equation

$$1 + z = \frac{dt_0}{dt_1} = \frac{a(t_0)}{a(t_1)} \tag{1.10}$$

Now let us return to the definition of the luminosity distance (1.1). In a flat and static geometry luminosity distance, d_L, is equal to the proper distance, leading to

$$d_L = a(t_0)r_1 \tag{1.11}$$

r_1 being the coordinate at which the wavecrest of light is emitted. However, in an expanding universe the luminosity lessens by a factor of $(1 + z)^2$ since it is energy radiated per unit time and both energy and inverse time interval are redshifted by $(1 + z)$. Thus,

$$d_L^2 = a^2(t_0)r_1^2(1 + z)^2 \tag{1.12}$$

where r_1 can be linked to the emission time from Equation 1.6. For the three available k values, the $f_k(r)$ functions are

$$f_k(r_1) = c\int_{t_1}^{t_0} \frac{dt}{a} = \begin{cases} \sin^{-1}(r_1), & k = 1 \\ r_1, & k = 0 \\ \sinh^{-1}(r_1), & k = -1 \end{cases} \tag{1.13}$$

The values we get from the observations are the redshifts z, not t, so we need to replace dt with dz. For that, we take the derivative of (1.10);

$$\frac{dz}{dt} = -(1+z)H(z) \tag{1.14}$$

Hence, $f_k(r_1)$ becomes

$$c\int_{t_1}^{t_0} \frac{dt}{a(t)} = -c\int_{z}^{0} \frac{dz'}{a(z')(1+z')H(z')} = \frac{c}{a(t_0)}\int_0^z \frac{dz'}{H(z')} = f_k(r_1) \tag{1.15}$$

Inverting the function,

$$r_1 = f_k^{-1}\left(\frac{c\int_0^z \frac{dz'}{H(z')}}{a_0}\right) \tag{1.16}$$

So, d_L from (1.12) becomes [2]

$$d_L(z) = (1+z)a_0 f_k^{-1}\left(\frac{c}{a_0}\int_0^z \frac{dz'}{H(z')}\right) \tag{1.17}$$

Remember that, in reaching these results, we only used the assumption of the FRW metric, without mention of any theory of gravity.

It is possible to evaluate $a(t)$, given that a theory of gravity and the type of the fluids which are contributing to the content of the universe are determined. To judge the validity of the chosen model following method is applied. Using assumptions of the theory $a(t)$ is evaluated, then $d_L(z)$, luminosity distance, is calculated from Equation

(1.17), and compared against the data. In this thesis, we use the same approach as the Çamlıbel PhD thesis [3] and the Semiz&Çamlıbel paper [4] (henceforth referred to as the "previous work"), where we try to fit different families of functions to the data and construct $a(t)$ from the best fits. We can do this analysis without using any theory of gravity or making any assumption of the matter-energy content of the universe.

Compared to the previous work, we use a more recent, richer and better quality dataset (the Pantheon [5] as opposed to the Union 2.1 data [6]), a more modern fitting criterion (χ^2 probability as opposed to χ^2/d.o.f.) and in the second part, also an alternative theory to that of Einstein's General Relativity (GR), namely, Starobinsky's $f(R)$ model [7].

1.2. $f(R)$ theories

$f(R)$ theories of gravity come about by straightforward generalization of the Lagrangian in the Einstein-Hilbert action,

$$S = \int d^4x\sqrt{-g}f(R) \tag{1.18}$$

where g is the determinant of the metric and R is the Ricci scalar. One may righteously ask, why are we complicating the action and as a consequence the field equations for no apparent reason. However, there are some problems with GR. It is not renormalizable and, as a result, cannot be quantized. In 1962, De Witt and Utiyama showed that renormalization at one-loop force the Einstein-Hilbert action to have higher order curvature terms [8]. The $f(R)$ models may also be a cure for current models' inability to explain the cause of the accelerated expansion of the universe or the nature of dark matter. Gravity is the most dominant force at cosmological scales and, as a result, it is the force controlling the evolution of the universe. So modified gravity may remove the need for the existence of the dark energy. [9]

After the modification of the Einstein-Hilbert action, generalized Friedmann becomes, [10]

$$H^2 + \frac{kc^2}{a^2} + \frac{1}{f'}\left[f''H\dot{R} - \frac{c^2}{6}\left(f'R - f\right)\right] = \frac{8\pi G}{3c^2 f'}\rho \tag{1.19}$$

where H is

$$H = \dot{a}/a \tag{1.20}$$

Clearly, the above equation reduces to the standart Friedmann equation for $f(R) = R$.

Now in order to make use of our data we need above equation in terms of a and its time derivatives. So, we calculate R. With the FRW metric at hand,

$$ds^2 = -c^2dt^2 + a^2(t)\left[\frac{dr^2}{1-kr^2} + r^2(d\theta^2 + \sin^2\theta d\phi^2)\right] \tag{1.21}$$

we can set about calculating the connection coefficients and with them Ricci scalar. The Ricci scalar is

$$R = \frac{6}{c^2}\left(\frac{\ddot{a}}{a} + \left(\frac{\dot{a}}{a}\right)^2 + \frac{kc^2}{a^2}\right) \tag{1.22}$$

taking its derivative with respect to t

$$\dot{R} = \frac{6}{c^2}\left(\frac{\dddot{a}}{a} + \frac{\ddot{a}\dot{a}}{a^2} - 2\left(\frac{\dot{a}}{a}\right)^3 - 2\frac{kc^2\dot{a}}{a^3}\right) \tag{1.23}$$

1.3. The Starobinsky model

The function $f(R)$ we choose to use in this thesis was suggested by Starobinsky [7]. The function and its derivatives with respect to Ricci scalar are

$$f = R + \alpha R^2 \qquad f' = 1 + 2\alpha R \qquad f'' = 2\alpha \tag{1.24}$$

First putting our chosen $f(R) = R + \alpha R^2$ into the modified Friedmann equation;

$$\begin{aligned}\frac{8\pi G}{3c^2}\rho &= (1+2\alpha R)\left(\frac{\dot{a}}{a}\right)^2 + (1+2\alpha R)\left(\frac{kc^2}{a^2}\right) + 2\alpha\left(\frac{\dot{a}}{a}\right)\dot{R} - \frac{c^2}{6}\left(R + 2\alpha R^2 - R - \alpha R^2\right) \\ &= \left(\frac{\dot{a}}{a}\right)^2 + \frac{kc^2}{a^2} + 2\alpha R\left(\frac{\dot{a}}{a}\right)^2 + 2\alpha R\frac{kc^2}{a^2} + 2\alpha\left(\frac{\dot{a}}{a}\right)\dot{R} - \frac{c^2}{6}\alpha R^2 \end{aligned} \tag{1.25}$$

then, putting R and $\dot{R}$ into the above equation and arranging the terms

$$\begin{aligned}\frac{8\pi G}{3c^2}\rho = \left(\frac{\dot{a}}{a}\right)^2 &+ \frac{6\alpha}{c^2}\left(2\left(\frac{\dot{a}}{a}\right)^2\left(\frac{\ddot{a}}{a}\right) - 3\left(\frac{\dot{a}}{a}\right)^4 - \left(\frac{\ddot{a}}{a}\right)^2 + 2\left(\frac{\dot{a}}{a}\right)\left(\frac{\dddot{a}}{a}\right)\right) \\ &+ \frac{kc^2}{a^2} - 12\alpha\frac{k}{a^2}\left(\frac{\dot{a}}{a}\right)^2 + 6\alpha\frac{k^2c^2}{a^4}\end{aligned} \tag{1.26}$$

We will use this to plot energy density of the universe in terms of redshift z.

1.4. Outline of the thesis

This thesis will mostly be about the expansion of the homogeneous and isotropic universe. In the next chapter, we fit various functions to the supernova type Ia (SN Ia) data and by using the best fits among them, then we try to extract information about the expansion history of the universe. The goal is the acquisition of the most information with the least amount of assumptions. As in previous work, we use Einstein's Equations to derive conclusions about the content of the universe in the past according to General Relativity. Finally, we assume a $f(R)$ gravity model; we choose the above discussed Starobinsky model for this job, to see if it can eliminate the so-called "dark energy".

2. METHOD

2.1. Mathematical Framework

At the end of the 20th century; it was discovered, through the SNe Ia observations [11, 12], that the universe was expanding at an accelerating rate, which contradicts what one would expect from a universe that is dominated by matter on a Friedman-Robertson-Walker (FRW) framework running under Einstein gravity theory. To this day the cause of this acceleration is one of the biggest mysteries in cosmology. Among the candidate explanations, most noteworthy are the Cosmological Constant Λ, scalar field Dark Energy (quintessence [13], phantom [14]), modified gravity [15] and braneworld scenarios [16].

In short, through observations, it was discovered that the supernovae at a given redshift z are dimmer than what would be expected even in the case of an empty universe. This dimness sets the supernovae further away than expected in an empty universe, and because of the constant speed of light, further back in time. Also, from Eq. 1.10 it is clear that redshift gives the size of the universe at the time light is emitted, so the faintness pulls the bottom of the a vs t curve to the left, thus the acceleration.

In the original works [11, 12], they used a model which takes matter and Einstein's cosmological constant (as the agent causing the acceleration, with $p = -\rho$) as the components that make up the universe, i.e. ΛCDM model. In those works, the contributions of matter and cosmological constant were parametrized as Ω_M and Ω_Λ then for the assumed values of these parameters they conducted fits of the data to the $d_L(z)$ functions. The best fits they found showed that $\Omega_\Lambda - \Omega_M = 0.4$, picturing a universe dominated by the cosmological constant, or its generalization, the dark energy.

Since then, other models have been suggested. To determine the theory's parameters, they generally followed the same procedure; i.e. they calculated $a(t)$ from

the theory, then evaluated $d_L(z)$ using eq.(1.17), and checked it against the data to determine the reliability of the model.

But, the method of going from a $a(t)$ to $d_L(z)$ can be inverted. We can solve for $t(z)$, using Equation 1.17;

$$c\int_t^{t_0}\frac{dt'}{a(t')} = f\left(\frac{d_L(z)}{a_0(1+z)}\right) \tag{2.1}$$

Taking derivative with respect to z,

$$-c\frac{dt}{dz}\frac{1}{a(t)} = f'\left(\frac{d_L(z)}{a_0(1+z)}\right)\frac{1}{a_0}\frac{d}{dz}\left(\frac{d_L(z)}{1+z}\right) \tag{2.2}$$

Now replacing f' from [1.6] and $a(t)$ from [1.10] and rearranging terms we get,

$$t_0 - t = \int_0^z \frac{dz}{(1+z)c\sqrt{1-\kappa\frac{d_L^2(z)}{(1+z)^2}}}\frac{d}{dz}\left(\frac{d_L(z)}{1+z}\right) \tag{2.3}$$

where κ is defined as

$$\kappa = \frac{k}{a_0^2} \tag{2.4}$$

thus it is a parameter that can take continuous values.

Since SNe Ia data do not say anything about the curvature of the universe, we keep the curvature κ-term. Once we evaluate $t(z)$, we can invert it to get $z(t)$.

To continue with our analysis little modification to eq.(2.3) is needed. Because, what is measured is not exactly luminosity distance but the apparent magnitudes, m, of the supernovae. It is well known that the absolute magnitudes of all the SNe Ia are considered to be the same, since all of them explode at the same mass so we can find a value for $d_L(z)$ by assuming an absolute magnitude for type Ia supernova but we

refrain from doing so in order to keep our analysis model-independent.[1] So we define a new function and do our fits to it instead. Starting with the definition of the luminosity distance

$$d_L = 10^{(\mu/5-5)}\ \text{Mpc} = 10^{\left(\frac{m-M}{5}-5\right)}\ \text{Mpc} = 10^{-M/5}10^{\left(\frac{m}{5}-5\right)}\ \text{Mpc} \tag{2.5}$$

our new distance function, we name it uncalibrated luminosity distance, is (μ is distance modulus, M and m absolute and apparent magnitude respectively)

$$d_m \equiv 10^{\left(\frac{m}{5}-5\right)}\ \text{Mpc} = 10^{M/5}d_L \tag{2.6}$$

we use this in the rest of the analysis. Putting $d_m(z)$ into eq.(2.3), we get

$$t_0 - t = \int \frac{dz}{c(z+1)} \frac{1}{\sqrt{1-\frac{k}{a_0^2}10^{-2M/5}\frac{d_m^2(z)}{(z+1)^2}}} 10^{-M/5}\frac{d}{dz}\left(\frac{d_m(z)}{z+1}\right) \tag{2.7}$$

and defining $t_M = 10^{M/5}t$ we get

$$dt_M = -\frac{dz}{c(z+1)} \frac{1}{\sqrt{1-\frac{k}{a_0^2}10^{-2M/5}\frac{d_m^2(z)}{(z+1)^2}}} \frac{d}{dz}\left(\frac{d_m(z)}{z+1}\right) \tag{2.8}$$

This is another difference of the present work from the previous work, where an M-value of -19.3 was implicitly assumed by the use of the Union 2.1 data.

So, as long as we have a good grasp of the $d_m(z)$ function along with the analytical evaluation of the integration (2.3) and its ensuing inversion is doable, we would have a good candidate for the expansion history of the universe from Eq. 1.10. Then, taking derivatives of that function would give us the periods of acceleration and deceleration.

[1] Absolute magnitudes of Supernovae Type Ia are still not well-constrained and are often presented within a distribution of values deduced from cosmic distance ladder data [17]. Cosmological data, on the other hand, is only sensitive to their multiplication with H_0 [18]. Therefore we carry out our analysis without assuming a value for absolute magnitude as long as we can, and if we have to, we use the fiducial value of M=-19.3, as implicitly done in the Union 2.1 dataset."

Hence, we do the analysis like in the previous paper, only this time using our new function $d_m(z)$ instead of the $d_L(z)$. We fit various families of function to the $d_m(z)$ data and determine the best fitting member of each family. Our choice of function families is not because we have a physical model in mind, rather they are chosen to simplify the analytical operations. We think it is better motivated to look for good fits to $d_m(z)$ instead of $a(t)$, seeing that the observationally measured function is $d_m(z)$. Also, aside from the regular redshift z, we use other redshift variables, for reasons explained in the next section, and denote them as y_i. We also compare goodness of fit of the results with each other and additionally with the ΛCDM model.

From this, we try to obtain information about the expansion history of the universe, including periods of acceleration and deceleration. We find that not much progress can be made in terms of the time t, nevertheless both the first and the second time derivatives of $a(t)$, scale function, can be calculated analytically in terms of redshift variable y_i, once we figure out an analytical result for $d_m(y_i)$. Even though SNe Ia data are said to show that the current expansion of the universe is accelerating, in previous work it was found that this is a statement within the ΛCDM model; that the model-independent analysis of the Union 2.1 SNe Ia data alone cannot show us that the universe was decelerating in the past. To improve this situation GRB luminosity distance data [19] were also included in the fits, even though they are not exactly model-independent. Since they are much fewer in number and have very large errors, this model-dependence was judged not too much of a problem.

The acceleration history found by the same method from the Pantheon SNe Ia data are not as problematic as that in the previous work, hence the inclusion of the GRB data brings only slight improvement. Nevertheless, we do include them in this work, too.

2.2. Fitting the luminosity distance function

The traditional redshift variable z is not the only redshift variable available for use, depending on the work, it may not even be a good variable to work with. Cosmog-

raphy has generally been the attempt to get as many Taylor expansion coefficients as possible of diverse cosmological functions but looking at Eq. 1.10, it is clear that the radius of convergence of the Taylor series for $a(z)$ is 1, thus Taylor series may not work properly beyond $z = 1$ [20]. Hence, other redshift variables are used in the literature.

We will usually use y_0 in place of the traditional redshift z. The alternative redshift variables we will use are, as in the previous work,

$$y_1 = \frac{z}{1+z} \qquad y_2 = \arctan\frac{z}{1+z} \qquad y_3 = \frac{z}{1+z^2} \tag{2.9}$$

$$y_4 = \arctan z \qquad y_5 = \ln(1+z) \qquad y_6 = u = 1+z \tag{2.10}$$

where y_1-y_4 were introduced in [20,21], y_5 was introduced in the previous work and [22], and y_6 was used in the previous work, since it can suprisingly give different result despite its apparent triviality. We plot the different redshift variables in terms of scale factor

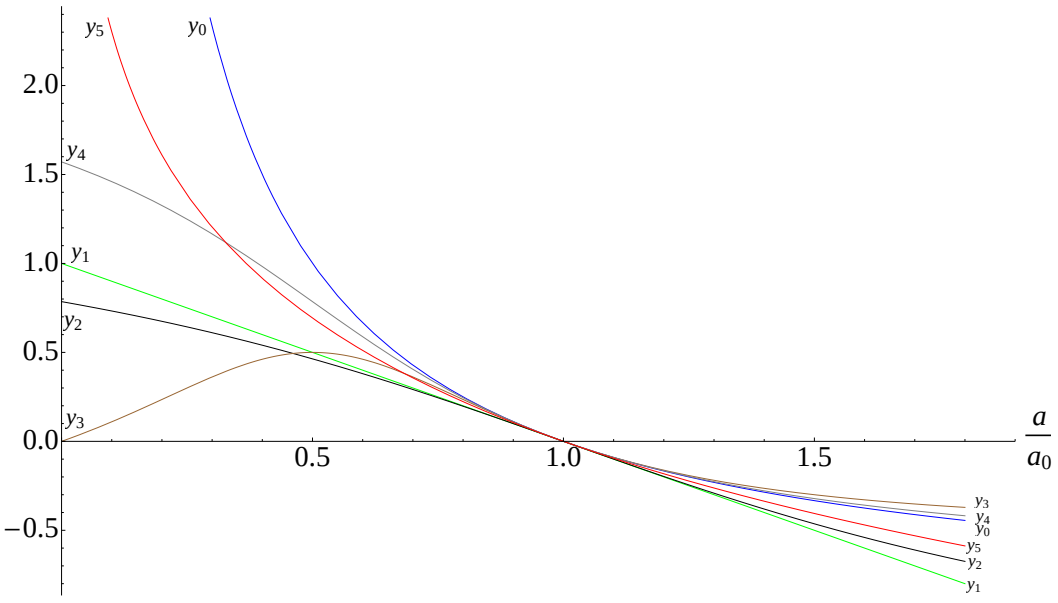

Figure 2.1. Relation between the redshift variables y_0-y_5 and the scale factor. Note that y_3 is not monotonic with a.

(Figure 2.1). As can be seen from this plot, y_3 does not change monotonically with scale factor, so it will not be used.

To find candidate functions for $d_m(y_i)$, we use 8 families of functions [See Table 2.1] to fit to the data, that is, Pantheon dataset. In each family one function is chosen as the best fit by looking at the χ^2 probability distribution of the fits. Since we want our analysis to be model-independent hence our function candidates need to be as generic as possible; therefore we begin with polynomials without constant term [except when using $y_6 = u = z+1$, when we determine the constant in terms of the coefficients of the other powers such that $d_m(u = 1) = 0$]. We get our second and third function families by multiplying them with an exponential function of which the exponent is linear and quadratic in y_i, respectively. We get the third, fourth and fifth function families by multiplying first three families by $(z + 1)$. One more generalization of polynomials is the Padé approximant [23–25] which is

$$\tilde{P}(y, M, N) = \frac{P_M(y_i)}{P_N(y_i) + 1} \tag{2.11}$$

where $P_M(y_i)$ is the M^{th} order polynomial without constant term, and again we generate one more family by multiplying Padé approximants by $(z + 1)$.

Table 2.1. The 8 different families used in fits. y can be any one of the redshift parameters described previously (y_0 to y_6), $P_N(y)$ is the N^{th} order polynomial with zero constant term (except when using $y_6 = u$), $u(y)$ is $(1 + z)$ expressed in terms of y, $\tilde{P}(y,\, M,\, N)$ is the Padé approximant in variable y and orders M & N; and c & d are constants.

Designation	Function family
F1	$P_N(y)$
F2	$P_N(y)u(y)$
F3	$P_N(y)\exp(cy)$
F4	$P_N(y)u(y)\exp(cy)$
F5	$P_N(y)\exp(cy + dy^2)$
F6	$P_N(y)u(y)\exp(cy + dy^2)$
F7	$\tilde{P}(y,\, M,\, N)$
F8	$u(y)\ \tilde{P}(y,\, M,\, N)$

In previous work, best fitting members are chosen by looking at their $\chi^2_\nu \equiv \chi^2/\text{d.o.f}$ value. This time, we choose the best fitting member of each family by maximizing their χ^2 probability. As a demonstration, in Figure 2.2 we plot the data in terms of the luminosity distance and standard redshift y_0 together with the $N = 2$ to 10 fits for the first family, the one-sigma confidence levels of the best fitting member of the first family, the curves of the flat matter-dominated model and the ΛCDM model. We can see that in Figure 2.2 that the matter-dominated curve is not a good fit so it is excluded, and the strange behavior of the high parameter curves ($N = 7$ to 10) can be explained by the overfitting to data.

We show the most useful function from each family in Figure 2.3, for the traditional redshift variable y_0. This time, we did not include the one-sigma confidence levels of the functions since doing so would render the figure illegible. And the Figures 2.4-2.8 are the same thing for other redshift variables.

All of the best fits of each family and redshift variable, together with their probability values are shown in Table 2.2. It seems that only two of the fits (F2,y_0), (F7,y_4) gives probability values worse than ΛCDM's 0.6780. Hence we will use all of the fits for the time being.

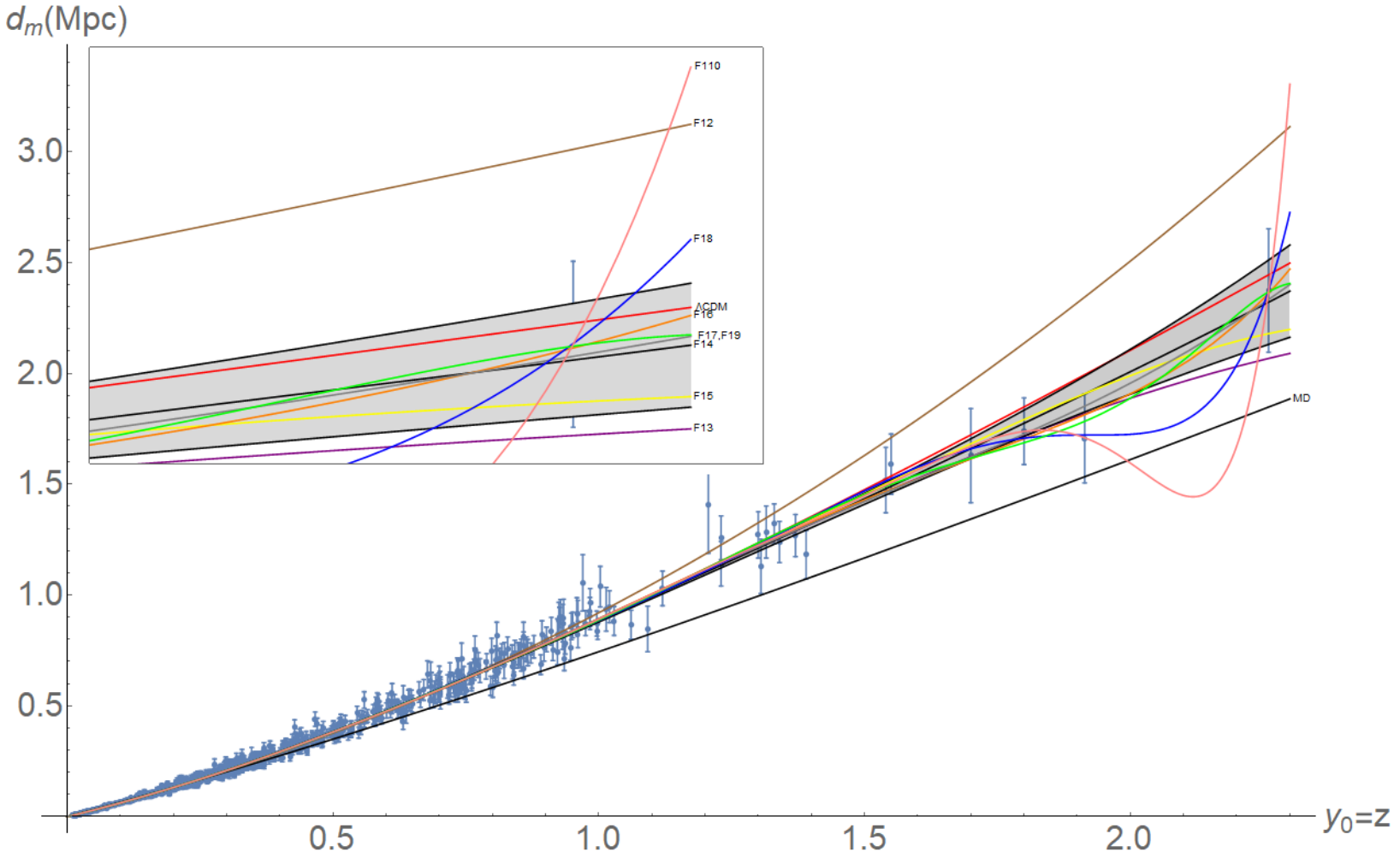

Figure 2.2. Pantheon data (in terms of uncalibrated luminosity distance and standard redshift $z \equiv y_0$); the N=2 to 10 fits for the first family, i.e. simple polynomials; the fits for the MD (black) and ΛCDM (red) models, and the one-sigma confidence-levels of the best-fitting member (N=4) of the family F1. The inset shows the right end, magnified.

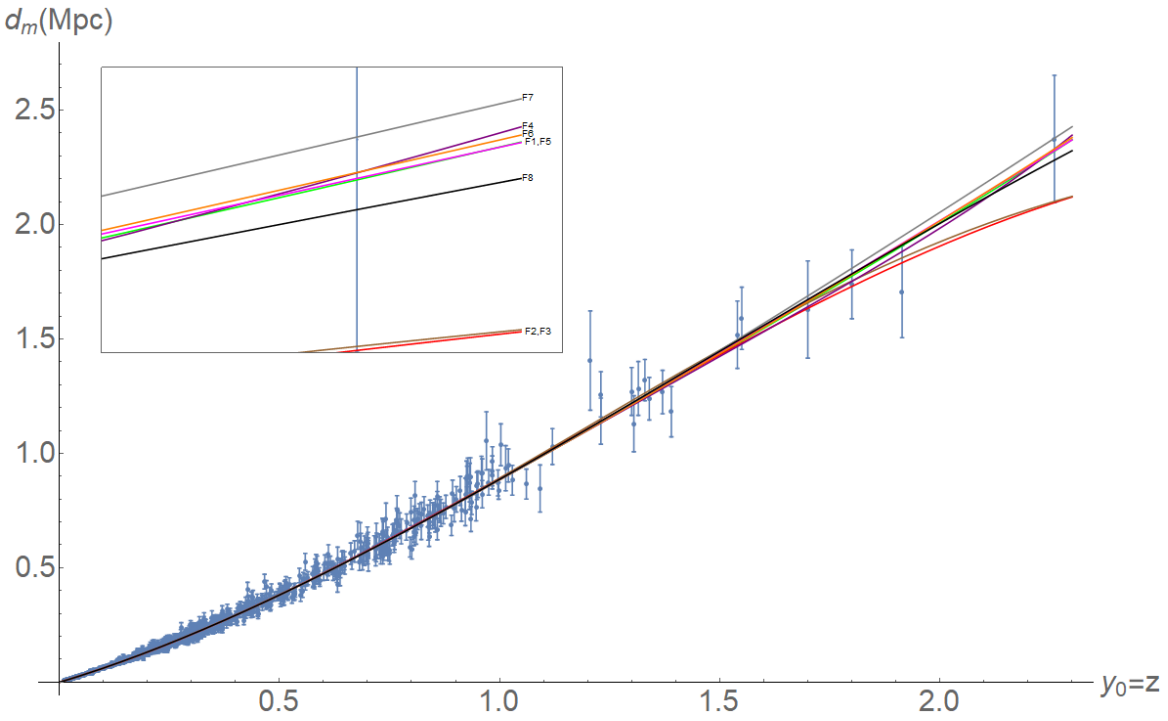

Figure 2.3. Pantheon data (in terms of uncalibrated luminosity distance and redshift $z \equiv y_0$); and best fits for each function family listed in Table 2.2. The one-sigma confidence-levels are not shown to not clutter up the figure; they are similar to those in Figure 2.2.

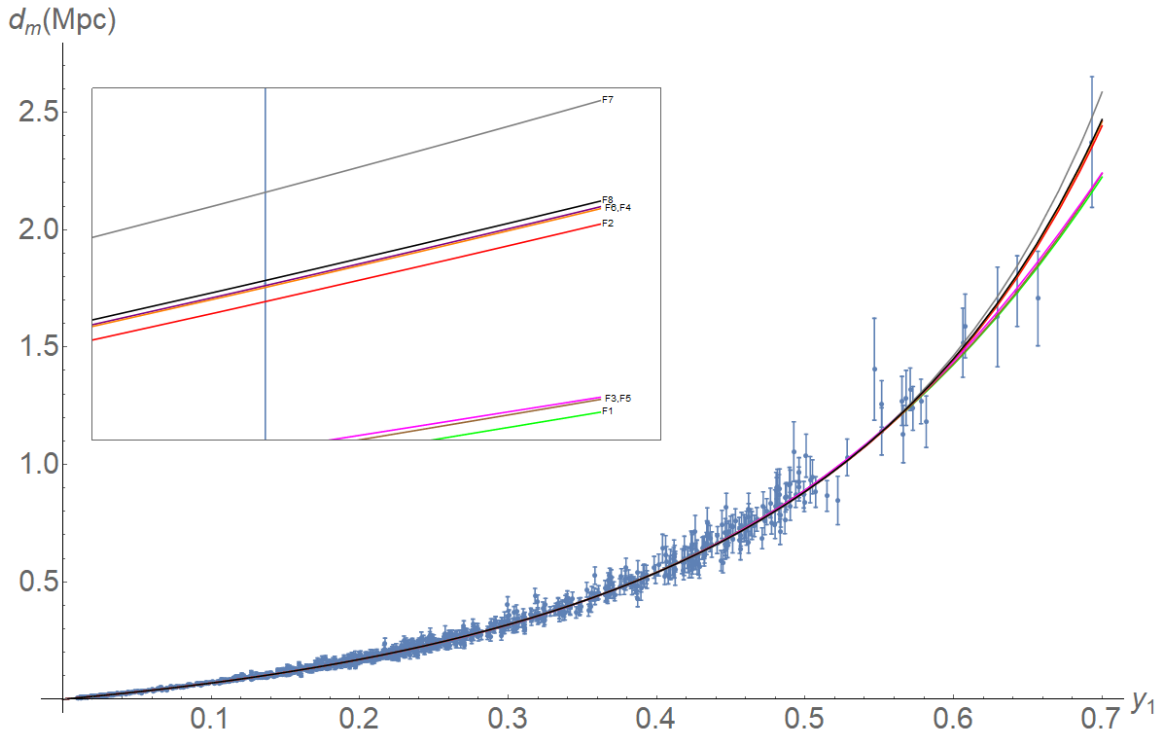

Figure 2.4. Same as in Figure 2.3 but with the redshift variable y_1.

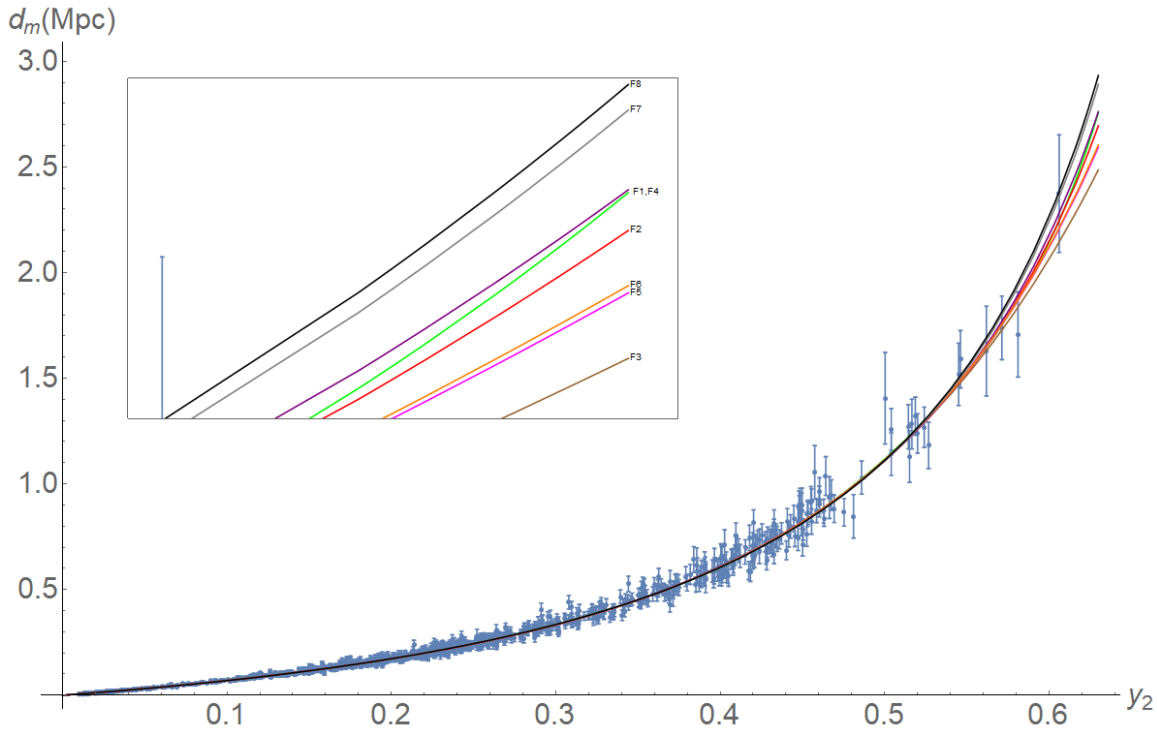

Figure 2.5. Same as in Figure 2.3 but with the redshift variable y_2.

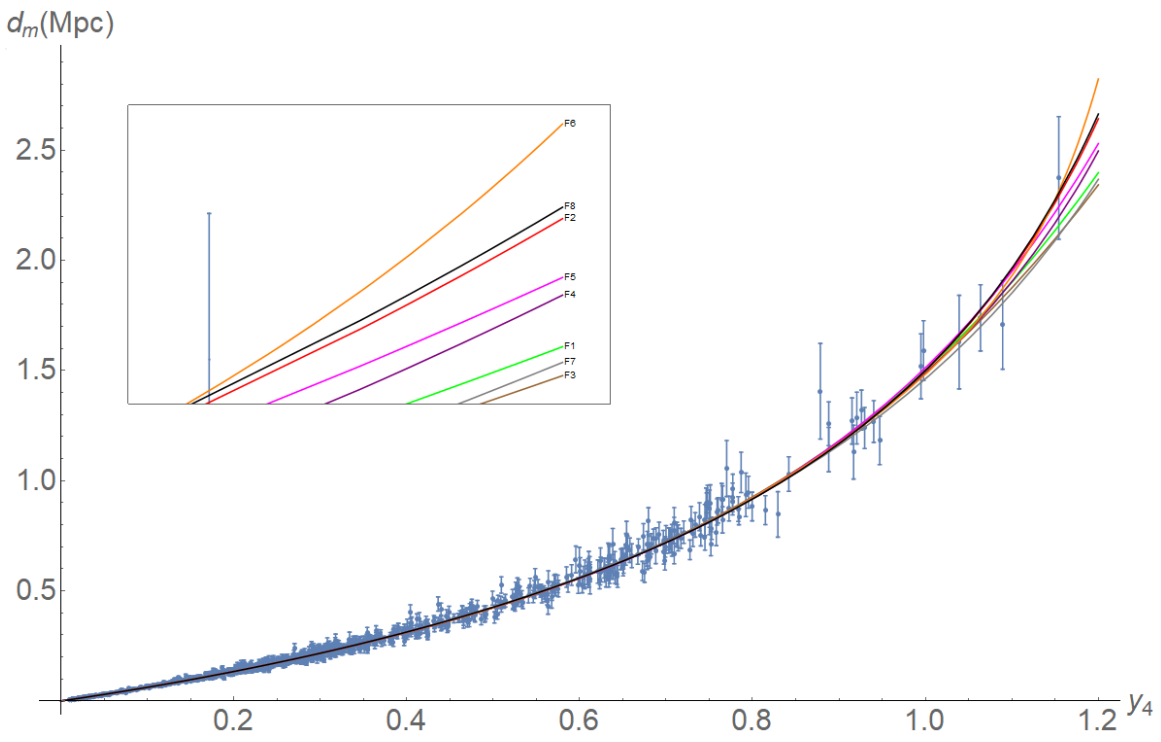

Figure 2.6. Same as in Figure 2.3 but with the redshift variable y_4.

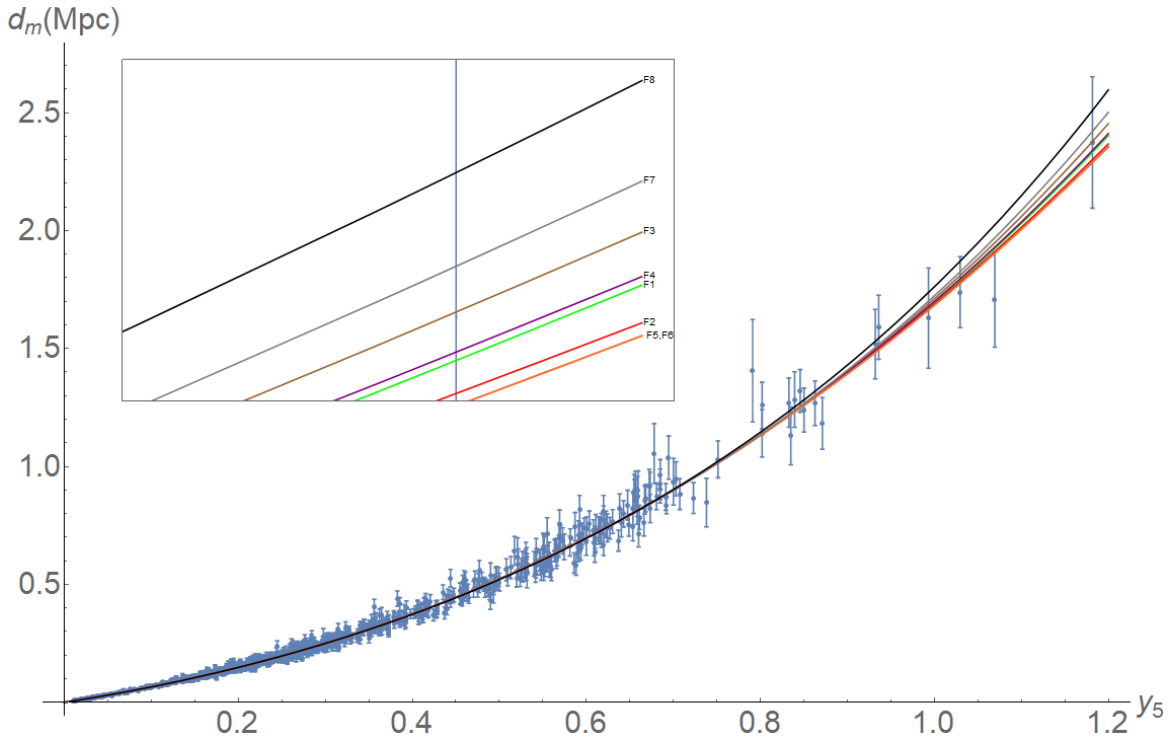

Figure 2.7. Same as in Figure 2.3 but with the redshift variable y_5.

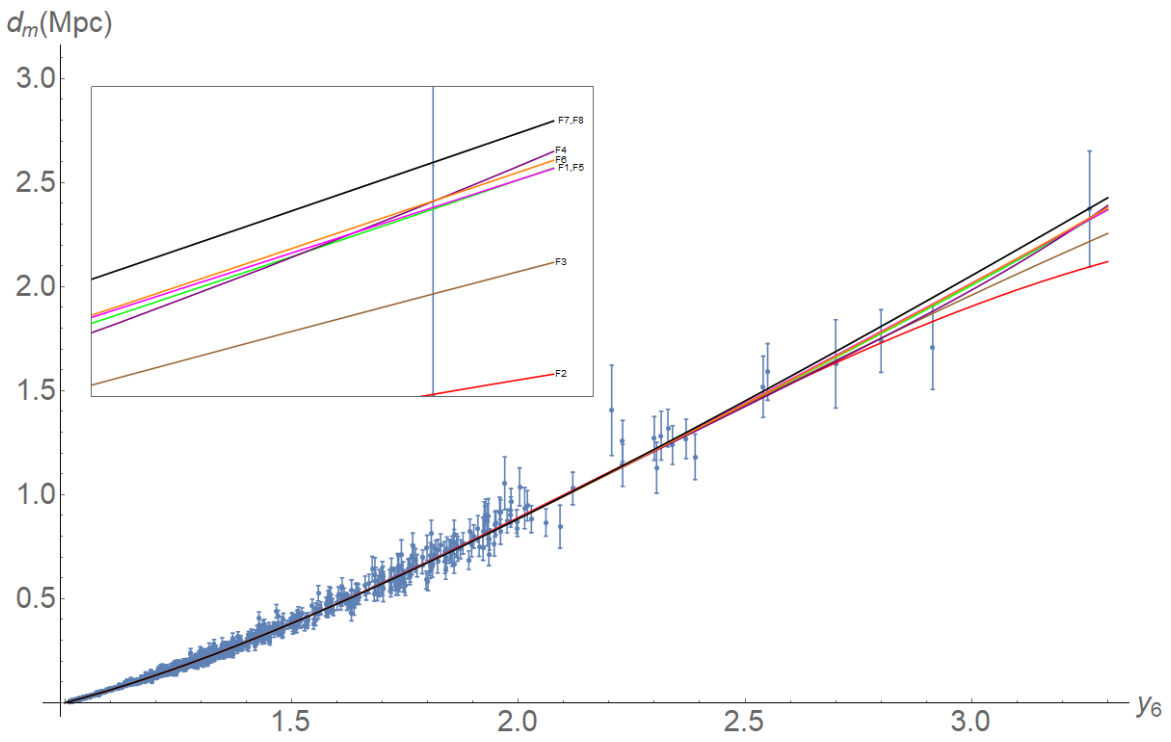

Figure 2.8. Same as in Figure 2.3 but with the redshift variable $y_6 = u = 1 + z$.

Table 2.2. The best fits for the Pantheon SNe Ia data. Each cell displays the internal label(s) of the best-fitting member of the row's family for the column's redshift variable, and the fit's χ^2 probability value. (The value for ΛCDM is 0.6780, using the redshift variable y_0, bigger is better).

variable / family	$y_0 = z$	y_1	y_2	y_4	y_5	$y_6 = u$
F1	4; 0.6903	4; 0.7310	9; 0.7540	4; 0.7140	3; 0.7012	4; 0.6903
F2	2; 0.6854	3; 0.6997	5; 0.7277	3; 0.6966	3; 0.7027	2; 0.6854
F3	5; 0.7044	5; 0.7238	5; 0.7199	5; 0.7075	3; 0.7028	3; 0.6970
F4	4; 0.6808	2; 0.7093	5; 0.7280	5; 0.7180	4; 0.6956	4; 0.6808
F5	4; 0.6931	5; 0.7220	4; 0.7323	4; 0.7152	3; 0.7002	4; 0.6931
F6	4; 0.6890	3; 0.7018	5; 0.7252	6; 0.7084	3; 0.7002	4; 0.6890
F7	2;1; 0.7024	2;1; 0.6936	1;2; 0.6982	2;1; 0.6389	2;1; 0.7005	2;1; 0.7024
F8	3;2; 0.7107	2;1; 0.7024	1;1; 0.7082	1;2; 0.6946	2;1; 0.6982	2;2; 0.6948

3. ANALYSIS AND RESULTS

3.1. Determination of the expansion history of the universe

As previously mentioned, what we want to do is to evaluate $t(z)$ by integrating eq.(2.8) for a given $d_m(z)$ function, then inverting that to get $z(t)$, then we can find $a(t)$ from eq. 1.10. Alas, neither the integration nor the following inversion can be analytically done, unless we use simplest functions. Although we can get numerical $a(t)$ functions by performing numerical integration and inversion, numerical differentiation of these is problematic, so it is not very useful.

However, the time derivatives of $a(t)$ can be evaluated analytically in terms of the redshift variables for a given $d_m(z)$ function, using the chain rule;

$$\dot{a} = \frac{da}{dt} = \frac{da}{dz}\frac{dz}{dt_M}\frac{dt_M}{dt} \tag{3.1}$$

defining,

$$\dot{a}|_M \equiv \frac{da}{dt_M} = \frac{da}{dz}\frac{dz}{dt_M} = 10^{-M/5}\dot{a} \tag{3.2}$$

similary for $\ddot{a}$ and $\dddot{a}$

$$\ddot{a}|_M \equiv 10^{-2M/5}\ddot{a} \quad \text{and} \quad \dddot{a}|_M \equiv 10^{-3M/5}\dddot{a} \tag{3.3}$$

One can easily see from the above equations that we need $\frac{dz}{dt_M}$ in order to plot $\dot{a}|_M$ and $\ddot{a}|_M$. At this point we use $M = -19.3$ to calculate $z(t)$ and since we can calculate $z(t)$ only by numerical integration, only plotting of $\dot{a}|_M(t)$, $\ddot{a}|_M(t)$ and $\dddot{a}|_M(t)$ are possible we cannot write them. However, $\dot{a}|_M$, $\ddot{a}|_M$, $\dddot{a}|_M$ can be analytically found as function of the used redshift variable, as will be seen below.

As mentioned, the SNe Ia data can be used for any value of curvature. When generating $\dot{a}|_M$, $\ddot{a}|_M$ and $\dddot{a}|_M$, we used Eq. 2.8, hence these functions will also contain the curvature κ. As in previous work, we choose $\kappa_0 = (10000\ \mathrm{Mpc})^{-2} \sim (2\mathrm{c}/\mathrm{H}_0)^{-2}$ as the upper limit to positive curvature. We do the analysis for 11 curvature values from $-\kappa_0$ to κ_0 with $0.2\kappa_0$ increments, i.e we take $\kappa = k'\kappa_0$, with $-1 \leq k' \leq +1$. This means that for every function and redshift variable there will be 11 curves.

3.1.1. Time derivatives of the scale function

We have 8 functions families, used together with 6 redshift variables to estimate $d_M(z)$ giving us 48 possible ways to show the expansion history of the universe. As in the previous work, plots for $a(t)$ are almost identical, so not very useful, hence we will omit them. Even tough the Pantheon data set contains about 500 more Type Ia data, plots of $\dot{a}$, $\ddot{a}$ and $\dddot{a}$ will be drawn from $z = 0$ to 1.5. The reason for this is that there are only six data points beyond $z = 1.5$ and only one beyond $z = 2$ (at $z = 2.26$); furthermore, plotting out to $z = 2.3$, even to $z \approx 7$ to the GRB region, introduced singularities for some of the $\dot{a}|_M(z)$, $\ddot{a}|_M(z)$, $\dddot{a}|_M(z)$ functions. The plots for $\dot{a}$ are shown in Figure 3.1. Most informative ones are the plots for $\ddot{a}$, shown in Figure 3.2, giving us the information about the periods of acceleration and deceleration. The plots for $\dddot{a}$ are shown in Figure 3.3, its plots are also not very informative.

Although irregularities of the $\ddot{a}|_M(z)$ are not as bad as they are in the previous paper, in which Union 2.1 dataset is used, they are still there. Hence, we will use the same cure which is the addition of the high redshift data, GRB data even though these are not really suitable for model-independent analysis; they are standardizable candles, not standard candles. They also have large errors compared to Pantheon data, which will give them little weight in the fits. From these low weights and the much smaller number of data, it can be concluded that the GRB data will not model-contaminate the analysis much. However, we only have the distance modulus (μ) of the GRB data so we need to calibrate it to make them compatible with apparent magnitudes of Pantheon

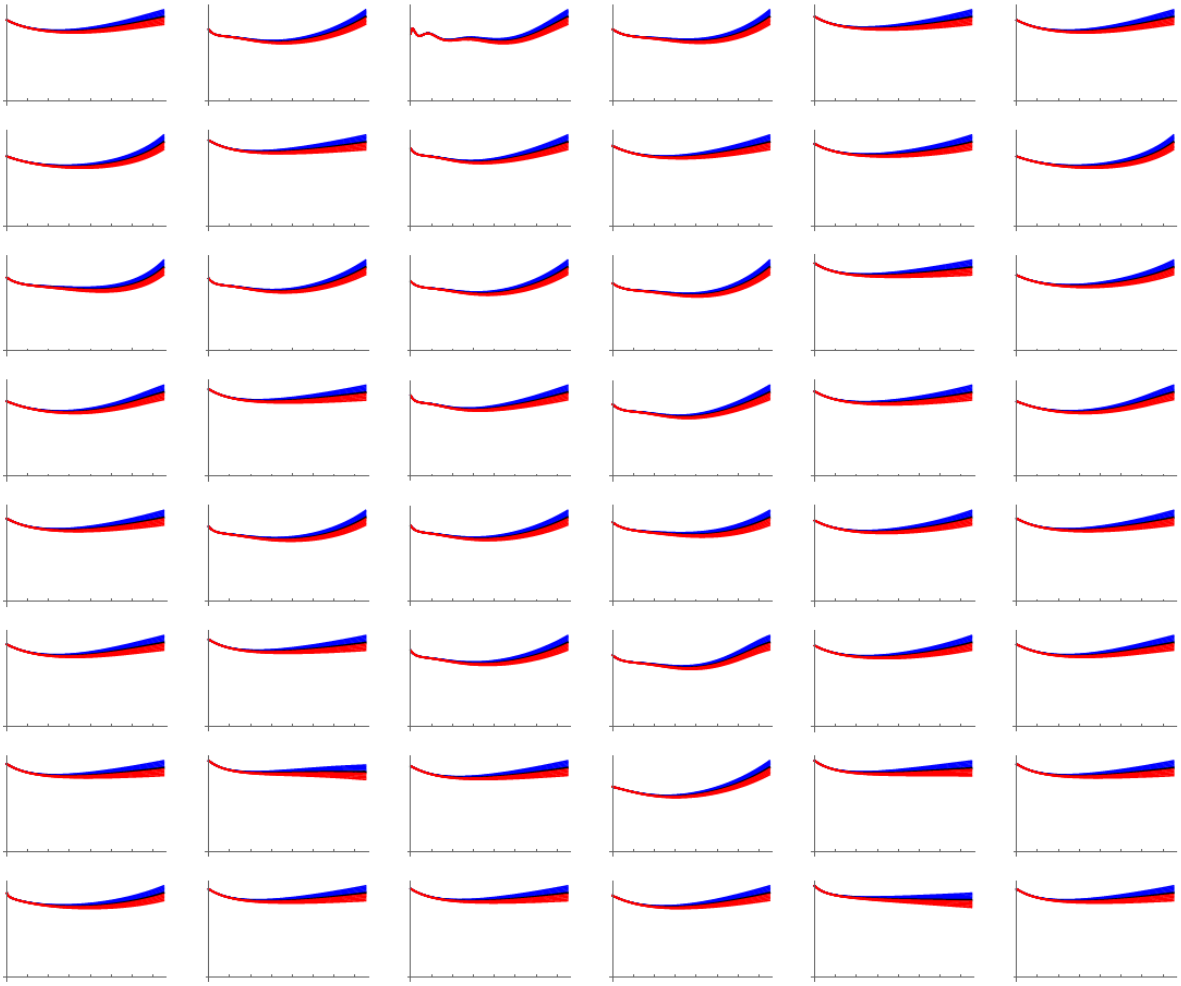

Figure 3.1. The $\dot{a}|_M(z)$ functions, computed analytically for the Pantheon data by Eq. 3.2 and similarly for y_i. The columns represents y_0 to y_6 and rows are for families F1 to F8. Blue, black and red curves are for open, flat and closed spaces respectively. To be able to compare them, horizontal axes are converted to y_0, ticked at intervals $\Delta z = 0.2$, and the vertical axes are in arbitrary units; cf. Figure 10 of [4].

data. Starting by putting them at the same luminosity distance.

$$\mu = m_s - M_s = m_g - M_g \tag{3.4}$$

where subscript s for supernova g for GRB.

$$m_s = m_g - M_g + M_s = \mu + M_s \tag{3.5}$$

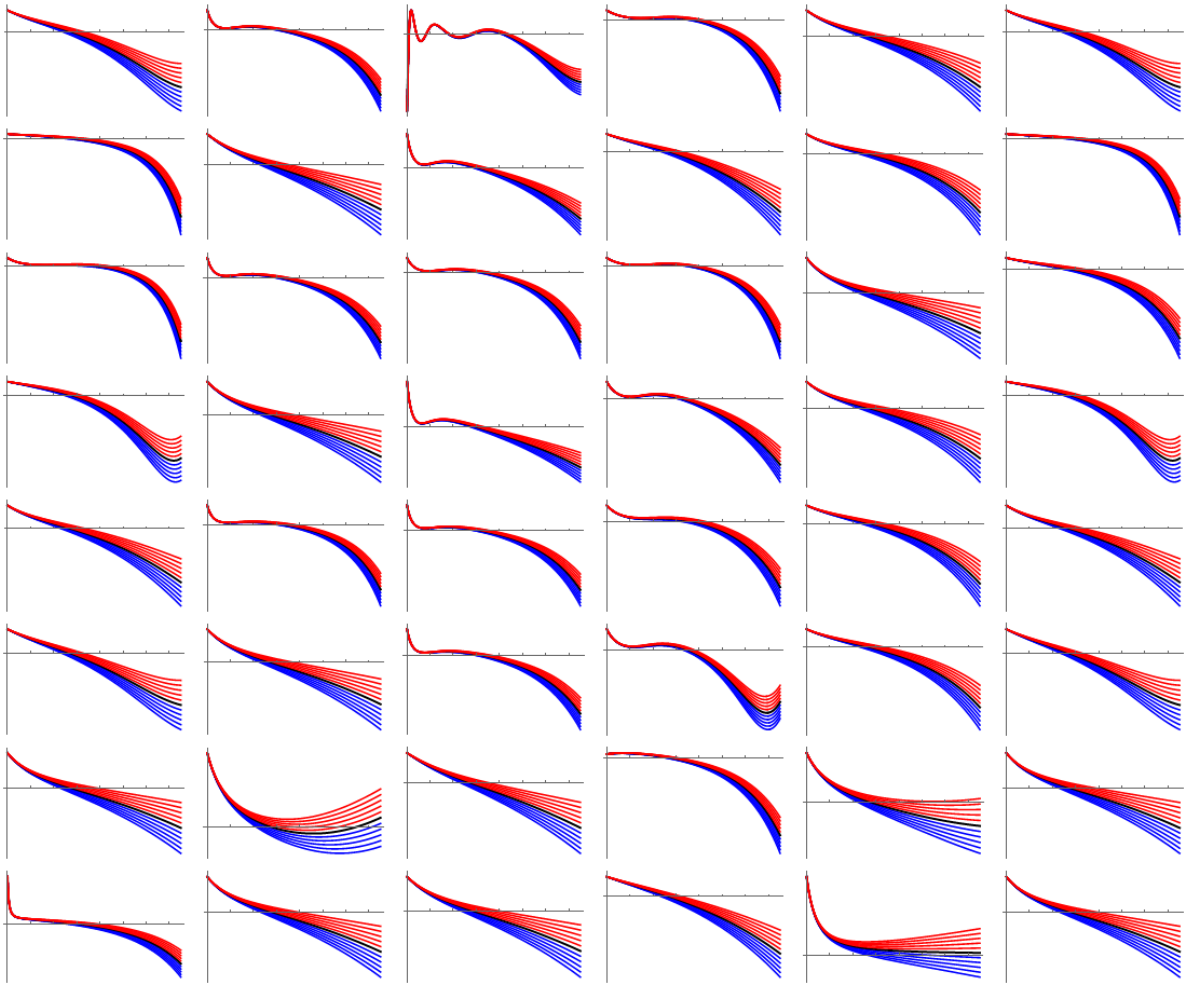

Figure 3.2. The $\ddot{a}|_M(z)$ functions, computed analytically for the Pantheon data by Eq. 3.3 and similarly for other redshift variables y_i. The columns, rows and colors are the same with the previous figure. Again, all horizontal axes are converted to y_0, ticked with intervals $\Delta z = 0.2$, and the vertical axes are in arbitrary units, hence, these could also be seen as plots of $\ddot{a}(z)$, to be compared to Figure 11 of [4].

Now the GRB data are like additional Type Ia SN data. We only need an absolute magnitude value for Type Ia, it is the same as the one we use previously to draw derivatives of scale factor ($M = -19.3$). The GRB data together with Pantheon data are shown in Figure 3.4.

Addition of 69 GRB data to 1048 Pantheon supernova data modifies the plots of $\ddot{a}|_M$ to give Figure 3.5; and the χ^2 probability values of the most useful functions in Table 3.1. Comparing Figure 3.2 to Figure 3.5 indicates that addition of GRB data is

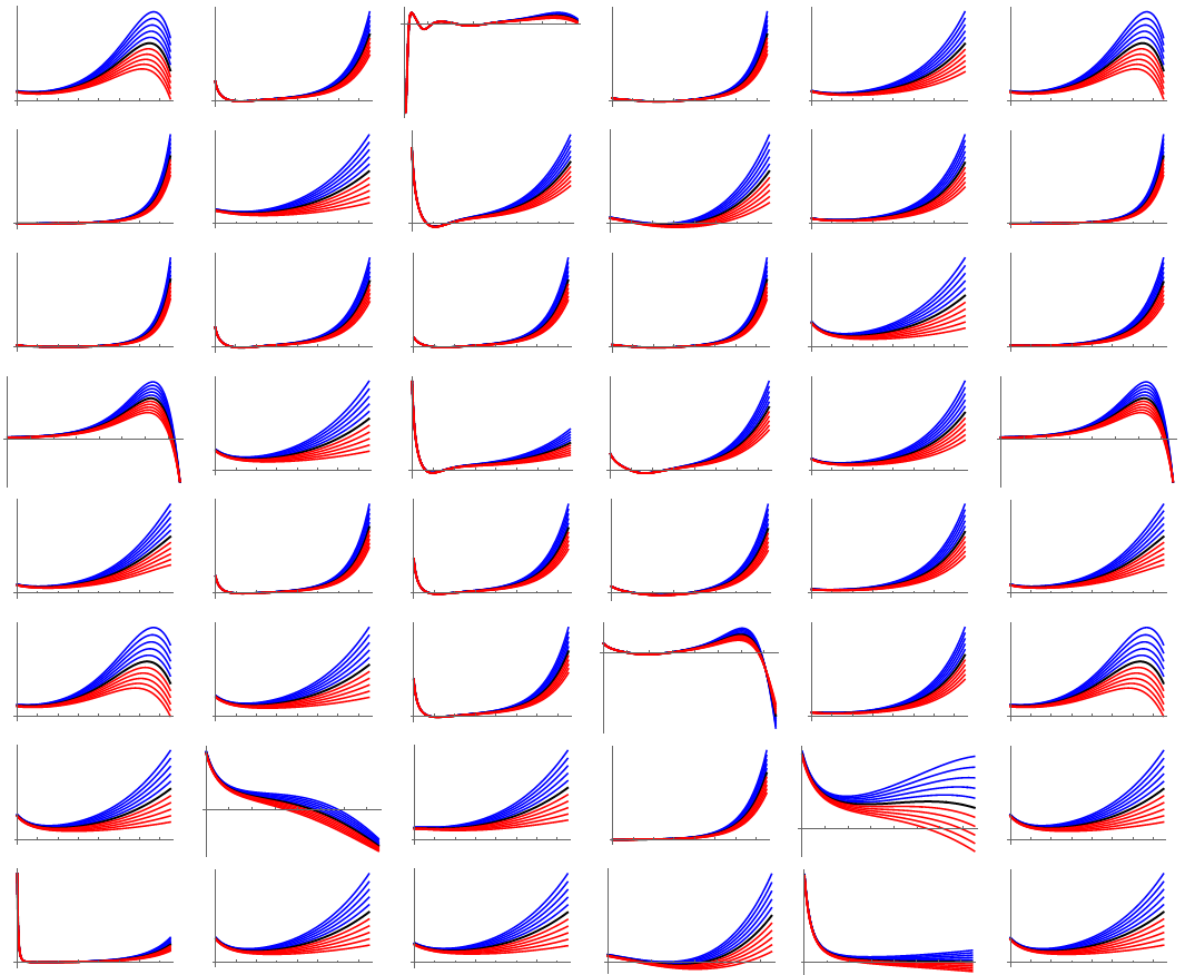

Figure 3.3. The $\ddot{a}|_M(z)$ functions, computed analytically for the Pantheon by Eq. 3.3 and similarly for other redshift variables y_i. The columns, rows and colors are the same as in figures 3.1-3.2. Again, all horizontal axes are converted to y_0, ticked with intervals $\Delta z = 0.2$, and the vertical axes are in arbitrary units, hence, these could also be seen as plots of $\ddot{a}(z)$.

not as useful as in previous work. But the difference is more apparent when we look at those graphs at higher redshifts; however, we plot only up to $z = 1.5$, as explained in the beginning of this subsection. Still, even for this range, the addition of GRB data was not for nothing. The number of plots in which we can see the transition from deceleration to acceleration clearly, increased. Additionally, there is a visual improvement to the plots of columns representing y_0, y_5 and y_6, they do not have any unnatural fluctuations. Strangely, adding the GRB data make columns representing y_0, y_5 and y_6 better but they make columns representing y_1, y_2 and y_4 even worse. As for functions from family F1, they do not give satisfactory result in either case.

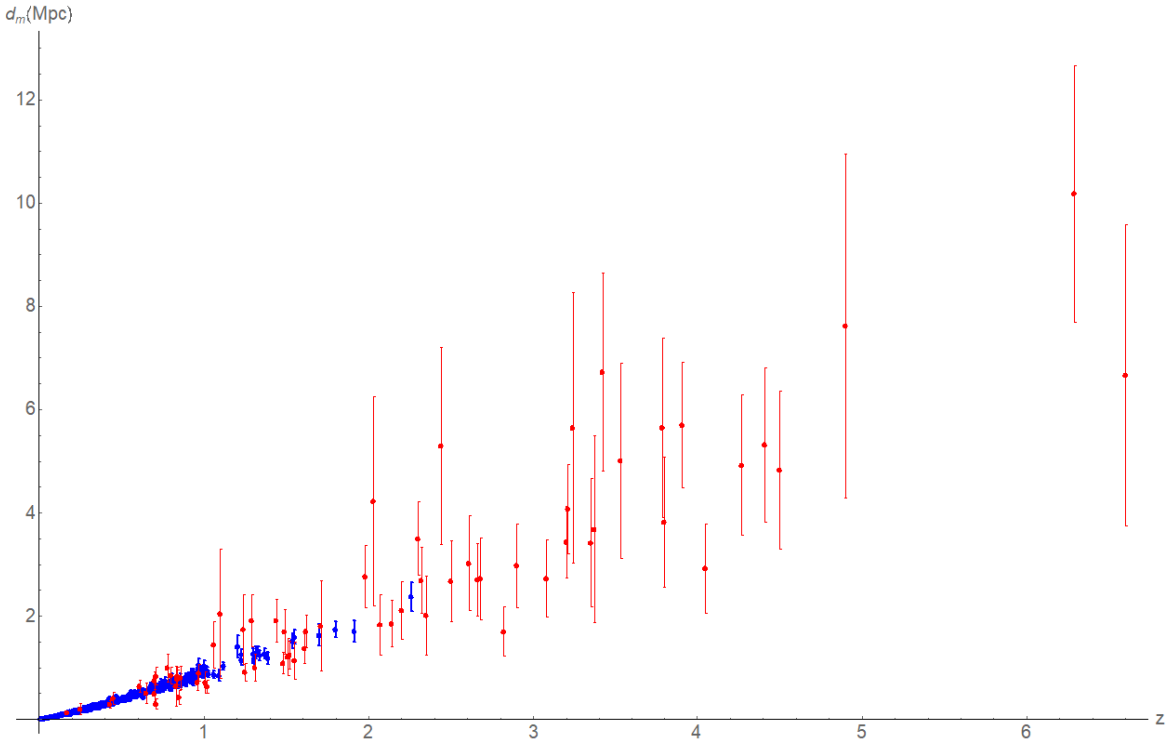

Figure 3.4. The Pantheon supernova data, shown in blue, the GRB data [19], shown in red, together.

Since, we have now data points up to $z = 7$, we also looked at the plots of $\dot{a}|_M(z)$, $\ddot{a}|_M(z)$ and $\dddot{a}|_M(z)$ functions up to redshift values of seven. Unfortunately, maybe because of the high error values of the GRB data or their low numbers, we got many plots with singularities. Only as a demonstration of said singularities, we show the plots of $\ddot{a}|_M(z)$ up to that point in Figure 3.6.

So, from this point on, we decided to discard the fits belonging to columns two, three and, four and row one of Figure 3.5. We show the average of the remaining 21 graphs in Figure 3.7. We compared all the 21 plots to this average one by one, to choose the one that is closest to it by minimizing the integral of the absolute value of the difference. The function we found was the one with redshift variable $y5$ and function family F8. We work with this in the subsequent sections.

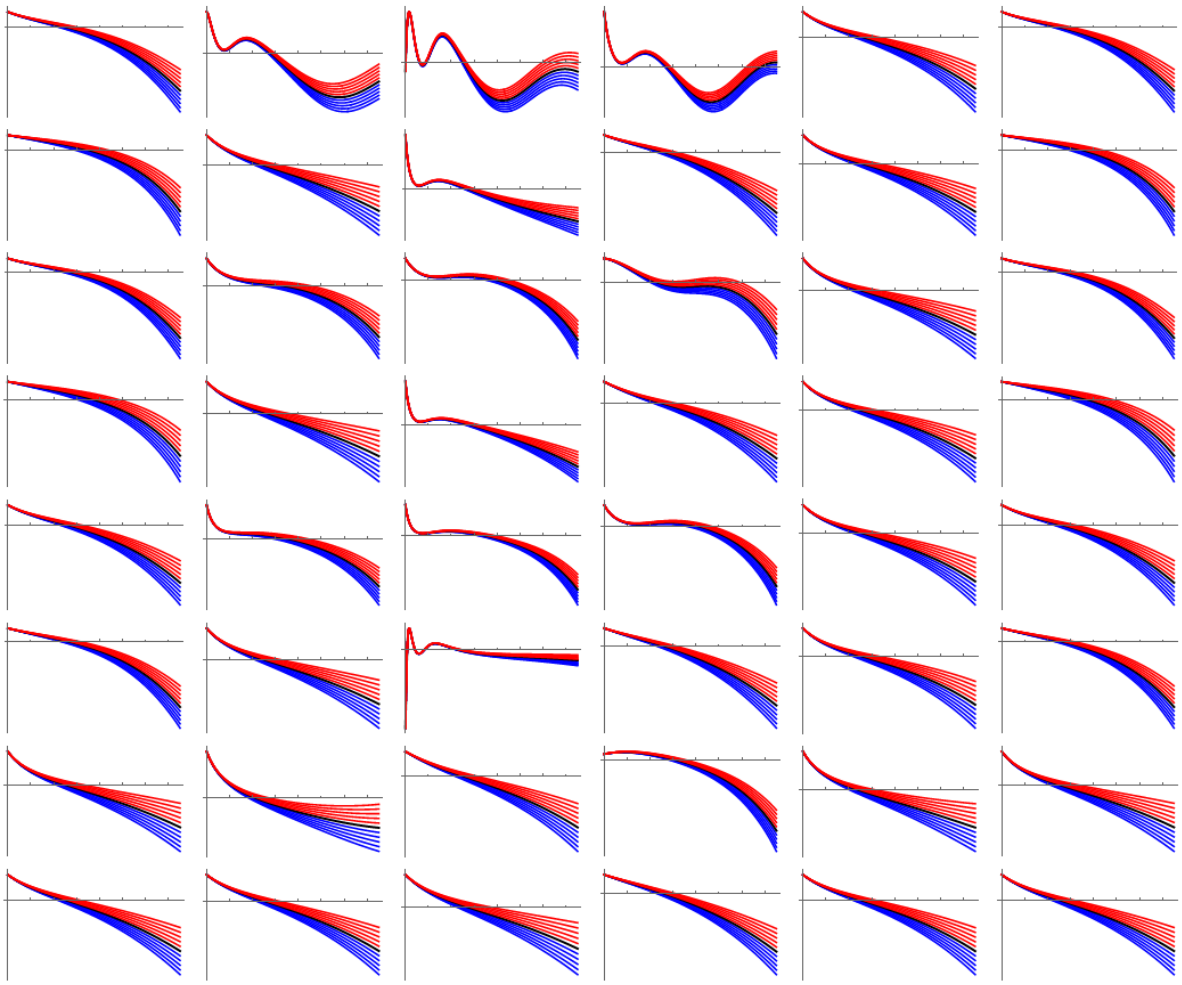

Figure 3.5. The $\ddot{a}|_M(z)$ functions, computed analytically for the Pantheon and GRB data by Eq. 3.3 and similarly for other redshift variables y_i. The columns, rows and colors are the same as in figures 3.1-3.2. Again, all horizontal axes are converted to y_0, ticked with intervals $\Delta z = 0.2$, and the vertical axes are in arbitrary units, hence, these could also be seen as plots of $\ddot{a}(z)$, to be compared to Figure 13 of [4].

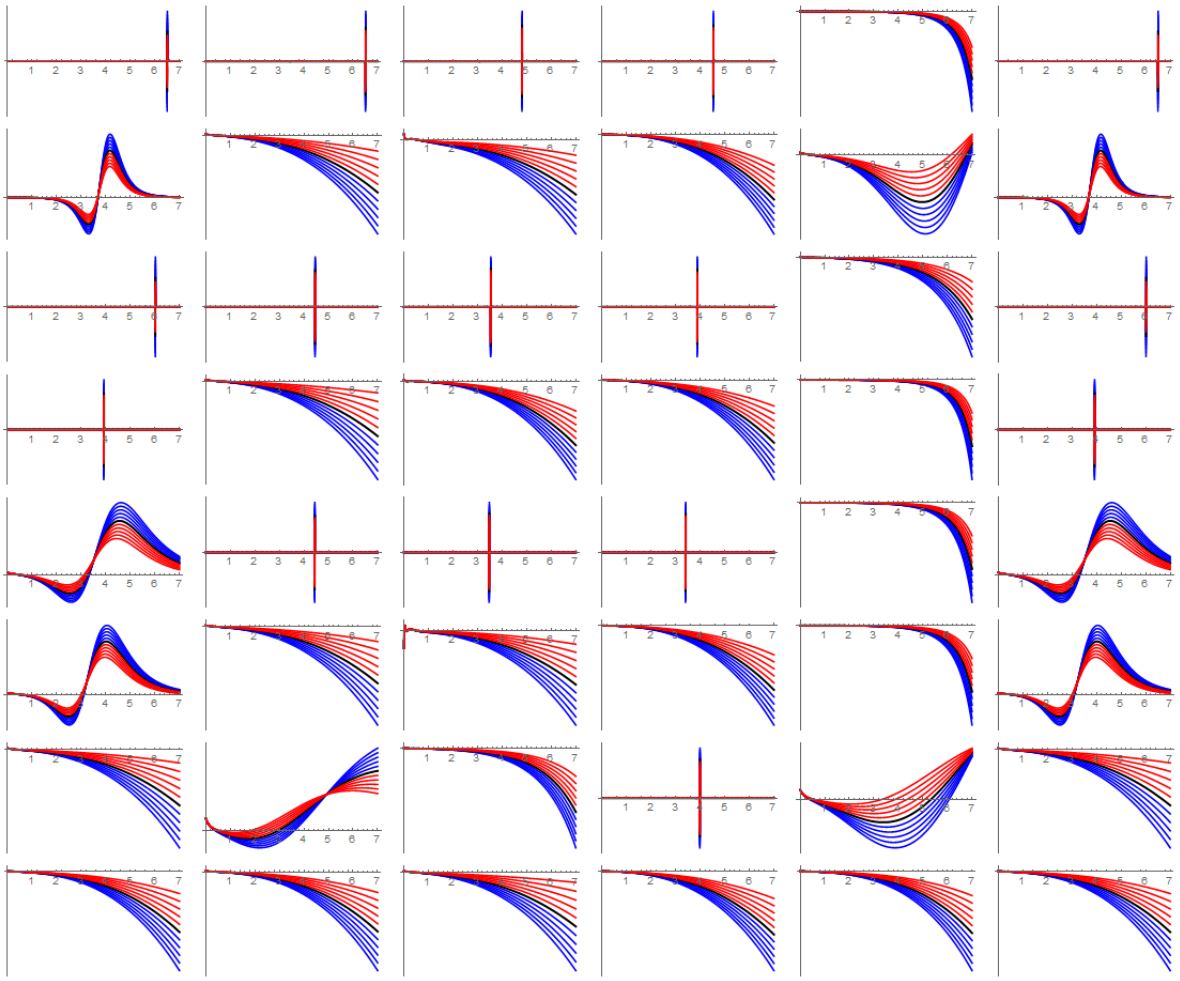

Figure 3.6. The $\ddot{a}|_M(z)$ functions, computed analytically for the Pantheon and GRB data by Eq. 3.3 and similarly for other redshift variables y_i. The columns, rows and colors are the same as in figures 3.1-3.2. Again, all horizontal axes are converted to y_0, and plotted up to $z = 7$, the vertical axes are in arbitrary units, hence, these could also be seen as plots of $\ddot{a}(z)$.

The redshift of transition from deceleration in the past to current acceleration, with its confidence interval, is

$$z_{t,\text{flat}} = 0.55^{+0.10}_{-0.07} \tag{3.6}$$

for flat universe,

$$z_{t,+} = 0.68^{+0.10}_{-0.12} \quad \text{and} \quad z_{t,-} = 0.46^{+0.07}_{-0.05} \tag{3.7}$$

for the most positively and negatively curved universes, respectively.

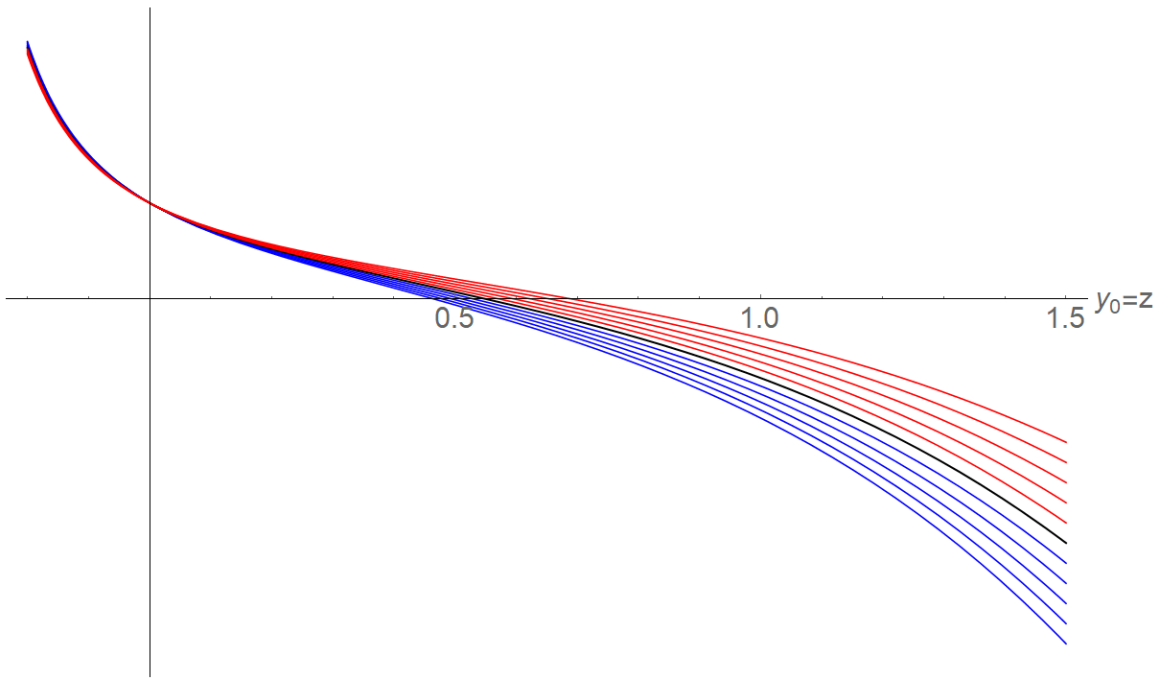

Figure 3.7. The average of the 21 "natural" $\ddot{a}|_M(z)$ functions from Figure 3.5, namely those in columns one, five and six, and rows two, three, four, five, six, seven and eight, extended to negative z, i.e. to the future. The color coding has the same meaning as in Figure 3.2. The horizontal axis shows $z = y_0$, ticked with intervals $\Delta z = 0.1$, and the vertical axis is in arbitrary units.

In Figure 3.7, we also show the part where redshift is negative predicting that the rate of acceleration will continue to increase in the future. But we do not feel justified to extrapolate very far into the future, given that fits usually behave strangely outside the data interval (and obviously we have no data of the future), so we plot only up to $z = -0.2$. All curves predict an increase in the rate of acceleration; some moderately, some more sharply.

Table 3.1. The most useful fits for the Pantheon SNe Ia + GRB data. Aside from the data used for fitting, everything is same with table 2.2.

family \ variable	$y_0 = z$	y_1	y_2	y_4	y_5	$y_6 = u$
F1	5; 06518	7; 0.6756	7; 0.6751	6; 0.6659	3; 0.6596	5; 0.6518
F2	3; 0.6072	3; 0.6584	6; 0.6834	3; 0.6559	4; 0.6537	3; 0.6072
F3	6; 0.6443	4; 0.6448	4; 0.6234	4; 0.6112	3; 0.6590	6; 0.6443
F4	2; 0.5698	2; 0.6617	5; 0.6865	4; 0.6516	4; 0.6523	2; 0.5698
F5	4; 0.6587	4; 0.6573	4; 0.6302	4; 0.6144	4; 0.6526	4; 0.6587
F6	4; 0.6518	3; 0.6585	7; 0.7153	3; 0.6557	4; 0.6526	4; 0.6518
F7	2;1; 0.6578	2;1; 0.6252	1;2; 0.6580	2;1; 0.5284	2;1; 0.6505	2;1; 0.6578
F8	2;2; 0.6524	1;2; 0.6602	1;1; 0.6583	1;2; 0.6555	2;2; 0.6526	2;2; 0.6524

3.2. Inferences in GR about the content of the universe

Now it is time to start using a gravity model in our work. We will start with General Relativity to see what it can tell us about the matter-energy content of the universe. Einstein's equation in FRW framework gives

$$H^2 + \frac{kc^2}{a^2} = \frac{8\pi G}{3c^2}\rho \tag{3.8}$$

hence it is straightforward to construct $\rho(z)$ using (3.2). We plot the energy density for different curvatures in Figure (3.8). Henceforth, we will be using d_L instead of d_M since a and $\dot{a}$ can only be calculated numerically by choosing an M value for SNIa. As explained in the previous section, this figure was created using the redshift variable $y5$ and function family F8.

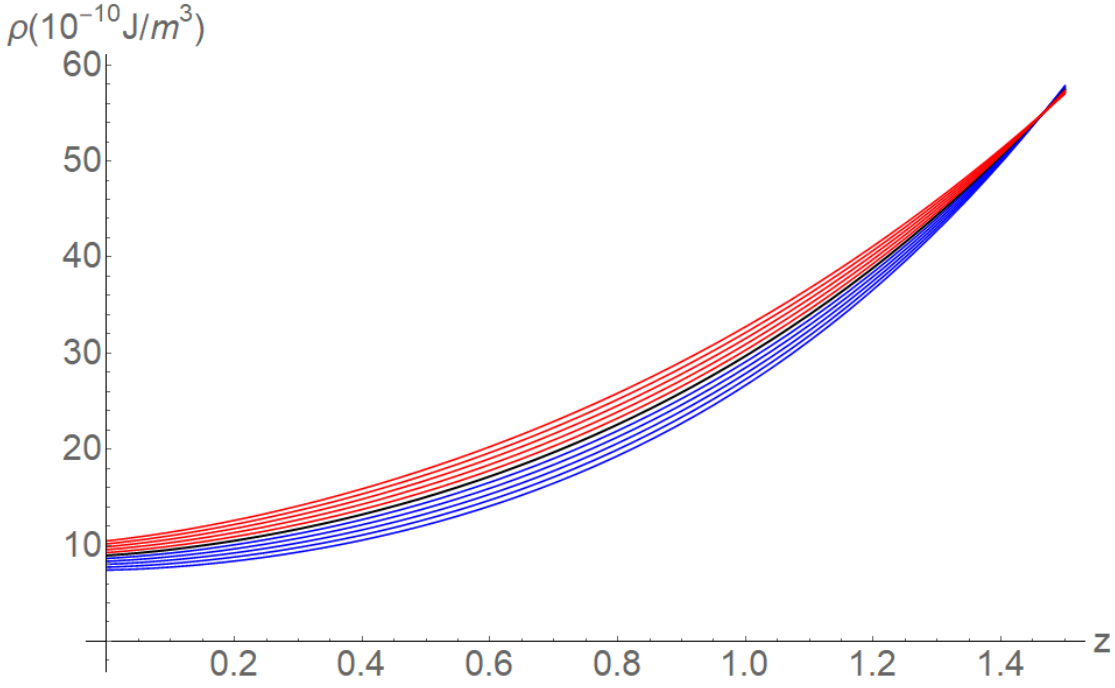

Figure 3.8. The density of the universe as function of z, as calculated using the redshift variable $y5$ and fit family F8, assuming Einstein gravity. The color-coding is the same as the one in Figure 3.1. Note the intersection around $z \approx 1.5$.

Note that in Figure 3.8 there is a specific value of redshift where the density is independent of the spatial curvature, i.e. there is an intersection point of all the plots,

as in previous work [4]. Even with the different dataset and function used, Figure 3.8 is almost same with the corresponding figure of the previous work. The analytical condition for the existence of this intersection point, called z_*, was derived in the previous work; it is not a condition that is obvious and always satisfied.

Nevertheless, as in the previous work, if we assume that all contributions to the energy density of the universe are positive, this intersection point, if/when it exists, will help us find an upper limit for the current value of matter density of our universe by equating the found density to the energy density of the matter-dominated universe at $z = z_*$:

$$\rho_{0\mathrm{m,max}} = \frac{3c^4}{8\pi G}\frac{z_* + 1}{d_L^2(z_*)} \tag{3.9}$$

where $\rho_{0\mathrm{m,max}}$ is the value of the matter-only curve at $z = 0$. The matter-only curve, proportional to $(1 + z)^3$, is shown together with $\rho(z)$, from GR, in Figure 3.9. With above equation we can also calculate an upper bound for current value of the density parameter for matter, $\Omega_{0m,\mathrm{max}}$. The results for the 21 $d_L(z)$ functions are given in Table 3.2. Similarly with the previous work y_5 variables gives more consistent values of z_*, hence $\Omega_{0m,\mathrm{max}}$.

From the previous work, the total current density of the universe is

$$\Omega_0 \approx 1 + 0.18k' \tag{3.10}$$

Since contribution of the radiation to the current density of the universe is negligible, the gap between Ω_0 values and the numbers in Table 3.2 indicates an existence aside from matter and radiation. The lower limit on the current density of this substance is

$$\Omega_{0,\mathrm{de}} \geq 0.32 \tag{3.11}$$

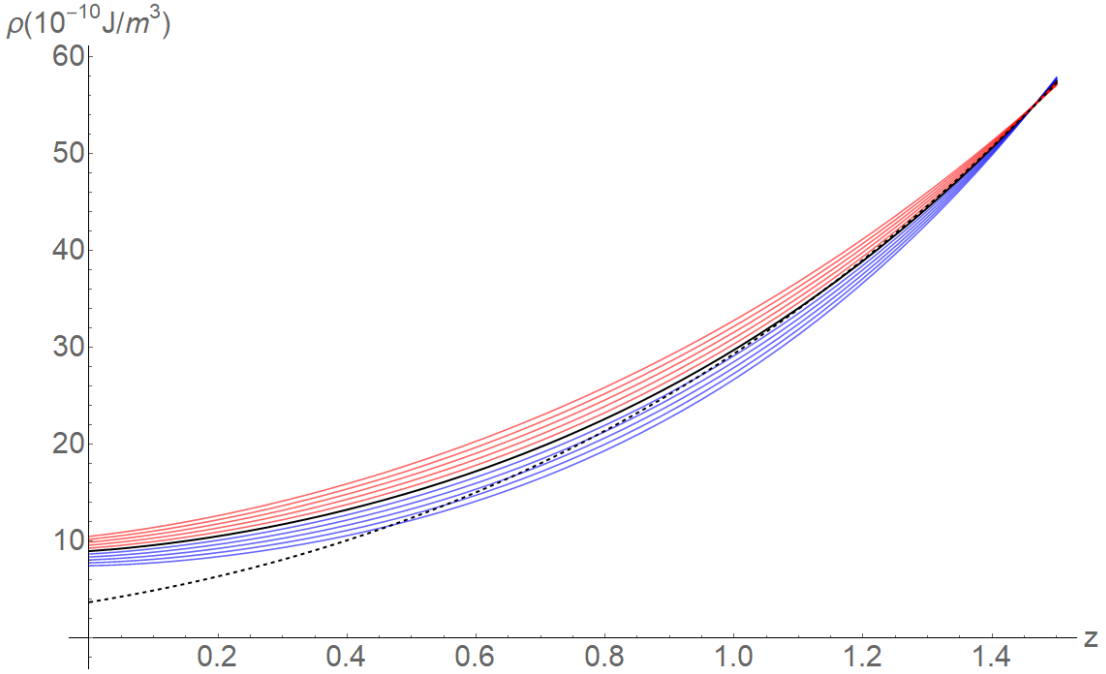

Figure 3.9. The density of the universe as function of z, as calculated using the redshift variable $y5$ and fit family F8, assuming Einstein gravity. The color-coding is the same as used in Figure 3.1. The dashed curve shows matter density, passing through the intersection point.

Table 3.2. z_* and $\Omega_{0m,\max}$ with their estimated errors calculated for 21 different $d_L(z)$ functions and assuming Einstein gravity.

$d_L(z)$	z_*	$\Omega_{0m,\max}$
y0-F2	$1.49^{+0.03}_{-0.03}$	$0.393^{+0.019}_{-0.019}$
y0-F3	$1.37^{+0.05}_{-0.04}$	$0.470^{+0.034}_{-0.037}$
y0-F4	$1.54^{+0.02}_{-0.03}$	$0.365^{+0.020}_{-0.013}$
y0-F5	$1.42^{+0.05}_{-0.04}$	$0.438^{+0.030}_{-0.034}$
y0-F6	$1.39^{+0.04}_{-0.04}$	$0.457^{+0.032}_{-0.030}$
y0-F7	$1.51^{+0.04}_{-0.05}$	$0.386^{+0.026}_{-0.024}$
y0-F8	$1.46^{+0.06}_{-0.04}$	$0.414^{+0.028}_{-0.036}$
y5-F2	$1.48^{+0.04}_{-0.04}$	$0.402^{+0.027}_{-0.026}$
y5-F3	$1.50^{+0.05}_{-0.04}$	$0.391^{+0.027}_{-0.029}$
y5-F4	$1.49^{+0.04}_{-0.04}$	$0.396^{+0.026}_{-0.025}$
y5-F5	$1.48^{+0.04}_{-0.03}$	$0.401^{+0.022}_{-0.025}$
y5-F6	$1.48^{+0.05}_{-0.03}$	$0.401^{+0.022}_{-0.025}$
y5-F7	$1.51^{+0.05}_{-0.05}$	$0.387^{+0.030}_{-0.028}$
y5-F8	$1.46^{+0.05}_{-0.04}$	$0.414^{+0.028}_{-0.031}$
y6-F2	$1.49^{+0.03}_{-0.03}$	$0.393^{+0.020}_{-0.019}$
y6-F3	$1.37^{+0.05}_{-0.04}$	$0.470^{+0.034}_{-0.037}$
y6-F4	$1.54^{+0.03}_{-0.02}$	$0.365^{+0.013}_{-0.017}$
y6-F5	$1.43^{+0.04}_{-0.04}$	$0.432^{+0.030}_{-0.028}$
y6-F6	$1.39^{+0.04}_{-0.04}$	$0.457^{+0.032}_{-0.030}$
y6-F7	$1.51^{+0.04}_{-0.04}$	$0.386^{+0.026}_{-0.024}$
y6-F8	$1.46^{+0.06}_{-0.04}$	$0.414^{+0.028}_{-0.036}$

3.3. Inferences in the Starobinsky model about the content of the universe

This time we are going to use the Starobinsky's $f(R)$ model to investigate how it works with the data and to see if it can give us the energy density of a matter-dominated universe that accelerates without dark energy. Unlike GR model which only requires the first time derivative of scale factor for calculating $\rho(z)$, now we need the second and third derivatives as well and additionally we need to assume a value for α. After plugging $\dot{a}(z)$, $\ddot{a}(z)$ and $\dddot{a}(z)$ in Equation (1.26), we plot the $\rho(z)$ for the α values of $(\pm 10, \pm 10^2, \pm 10^3, \pm 10^4, \pm 10^5, \pm 10^6$ Mpc$^2)$ (Figure 3.11). In those figures, we see a significant difference from GR only for α values greater than $\sim (10^3)$ Mpc^2 and less than $\sim (-10^3)$ Mpc^2. As for α's greater and less than $+10^6$ Mpc^2 and -10^6 Mpc^2, respectively, energy density shows negative values, hence we exempt those α's (for -10^6 Mpc^2 and below, current energy density is also negative). By looking at the plots we see that it is safe to assume any value for α from -10^6 Mpc^2 to 10^6 Mpc^2. We examined this interval, in steps of $10^{0.2}$ to see if there is an alpha value, for which the Starobinsky model could give a universe without dark energy. To do so, we look for energy density curves that are closer to that of matter-only universe; first we choose an arbitrary ρ_{0m} for the matter-only energy density curve and then tried to find the corresponding α by minimizing the integral of the absolute value of the difference.

$$\int |\rho(\alpha, z) - (j\rho(\alpha, 0) + \rho(\alpha, 0))(1+z)^3| \tag{3.12}$$

We look for the α and j values that minimize this integral. Simply put, we kept varying the current value of the matter-only curve (j) and α until we made the area between matter-only curve and curve of $\rho(z)$ as small as possible. We did this only for flat universe.

As a result, we see that none of the positive α values gave results better than GR ($\alpha = 0$), which means that we cannot eliminate dark energy with $\alpha > 0$ (Figure 3.10). However, we found what we were looking for with negative α values; in that region, it is possible to construct $f(R)$-energy density curves that are similar to that of a matter-dominated universe. We got the best result for $\alpha = -10^{5.6}$ Mpc^2 and

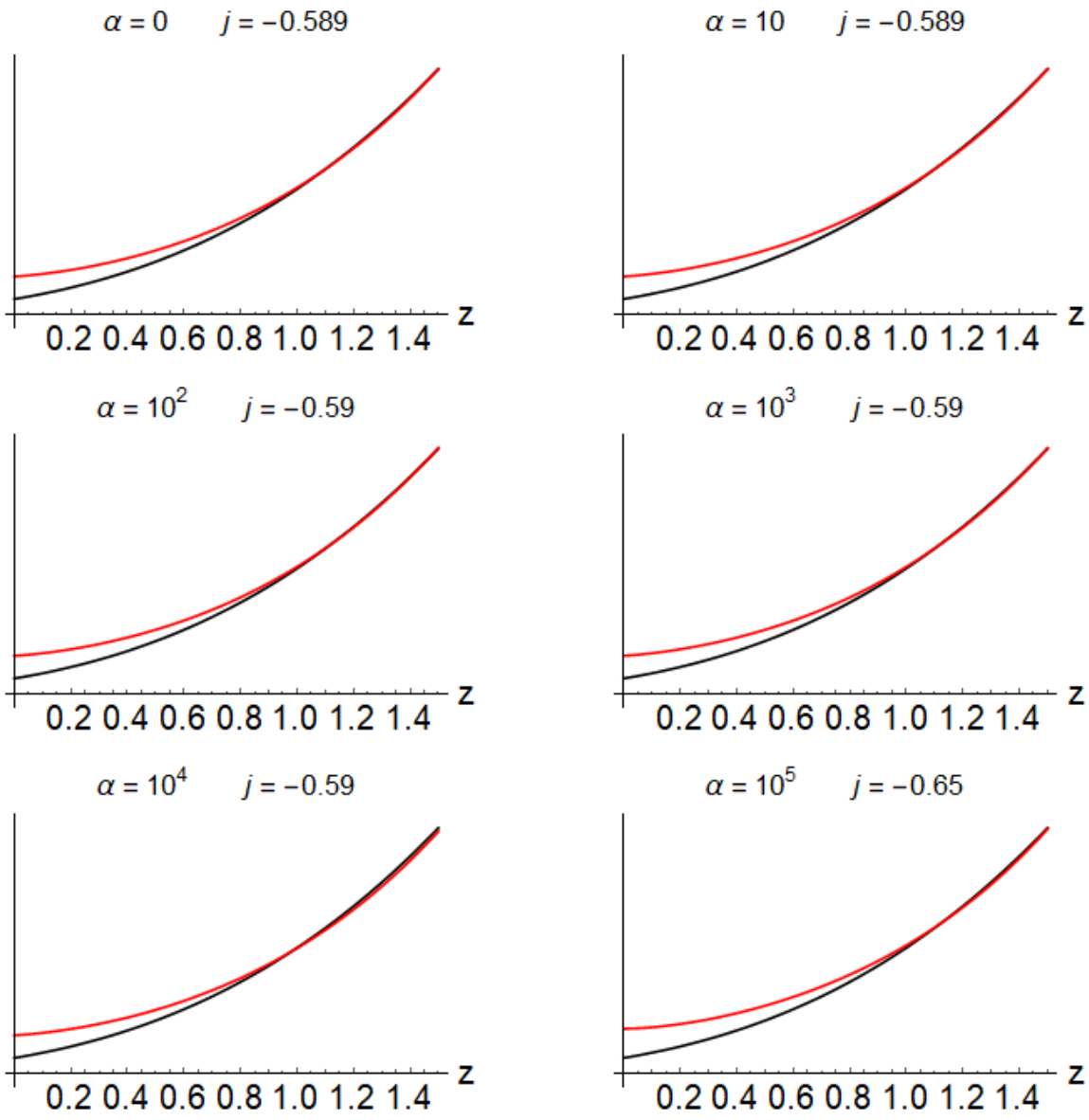

Figure 3.10. Matter-only density curve and $\rho(z)$ shown together for different α values (black is the matter-only curve). j values are those that minimize the Equation (3.12) for the chosen positive α values.

$j = -0.098$. The graph in which we compare $\rho(z)$ with matter-only curve (left panel) and plot of $\rho(z)$ together with varying curvatures (right panel) are shown in Figure 3.12.

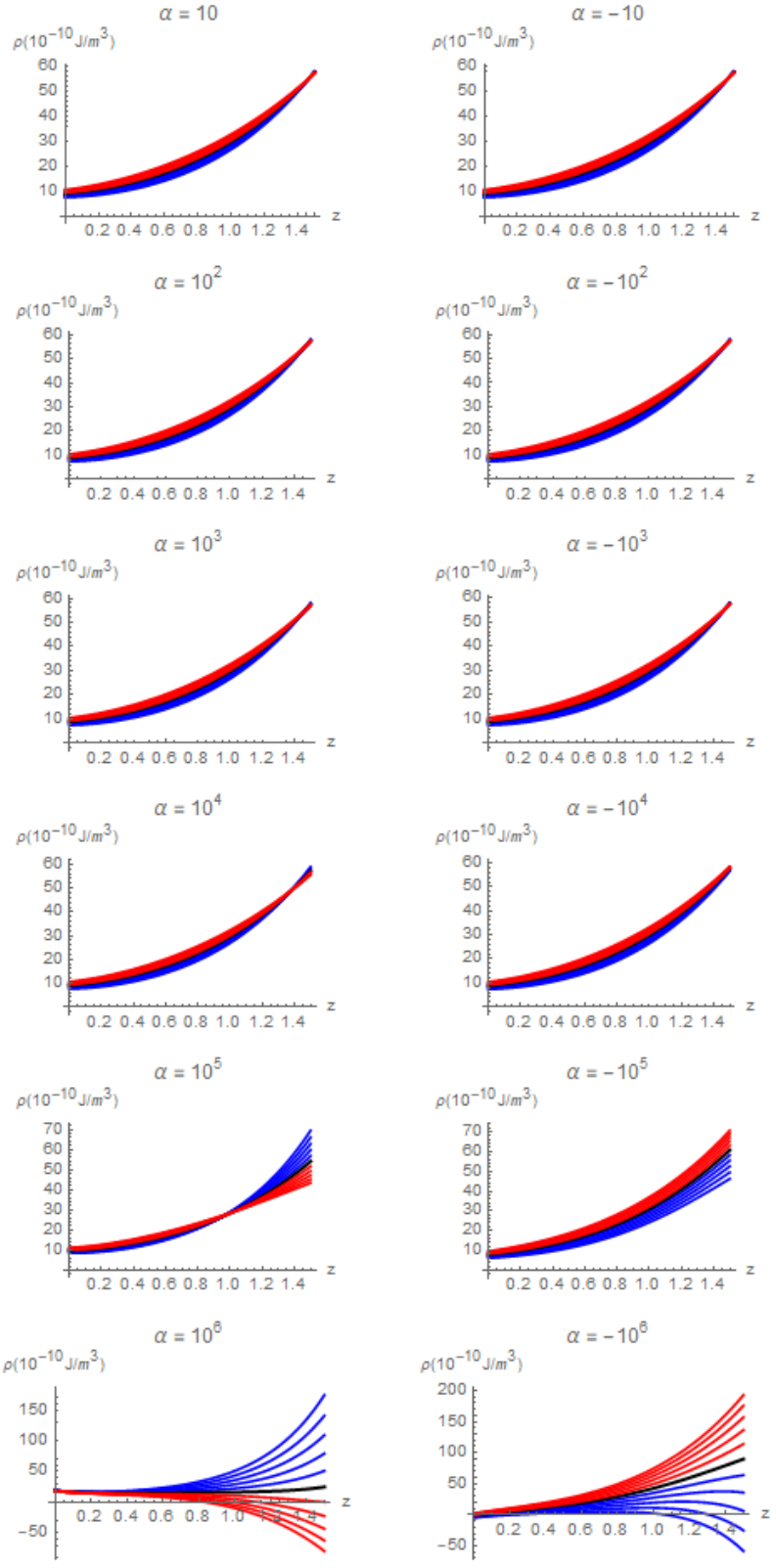

Figure 3.11. The density of the universe as a function of z, as calculated using the redshift variable $y5$ and fit family F8 for different α values, assuming Starobinsky's $f(R)$ model. The color-coding is the same as the one in Figure 3.1.

As hinted in Figure 3.12 we get negative energy density at high redshift values. For $\alpha = -10^{5.6}$ Mpc^2, for example, we start getting negative density values at around $z \approx 2.7$ for flat universe and even at smaller z for negative curvatures. This happens for every negative α, only the redshift value, at which the curves cross the axis, keep increasing as we got closer to $\alpha = 0$. (e.g. for $\alpha = -1$ Mpc^2, $z \approx 30$). Note that in

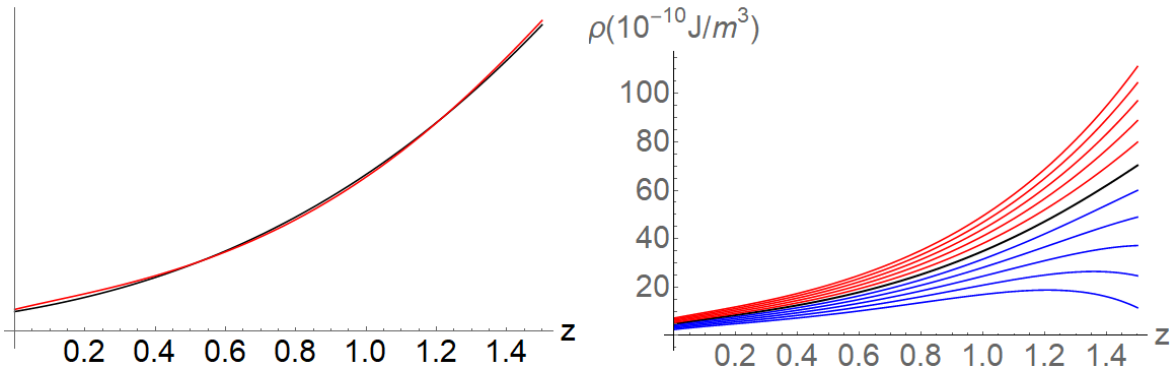

Figure 3.12. Matter-only curve ($j = -0.098$) and $\rho(z)$ shown together (black is the matter-only curve) in graph at left panel. Graph at right panel is the plot of $\rho(z)$ for $\alpha = -10^{5.6}$ Mpc^2, the color-coding is the same as used in Figure 3.1.

Figure 3.12, we no longer have the intersection point, $z*$, which we had in GR (Figure 3.9). We lose those points for α values smaller than $-10^{4.3}$ Mpc^2 and bigger than $10^{5.8}$ Mpc^2. Hence we cannot do the same $z*$ analysis that was done in Section 3.2. However, we can still find total current denstiy parameter using the left panel of Figure 3.12 and critical density from GR. This gives $\Omega_0 = 0.55$. From this result, we see that we have twice as much dark matter as compared to the ΛCDM model.

4. CONCLUSION

We started our analysis by fitting various functions to the uncalibrated luminosity distance (d_m), from the Pantheon Type Ia supernovae data compilation, and tried to get information about the expansion history of the universe. Form of the functions we used was chosen, as in the previous work, to make the transition from $d_m(z)$ function to $a(t)$. We first increased the number of parameters of the $d_m(z)$ functions we used, forming families, and from each family, we chose the one with the biggest χ^2 probability value. We fitted functions to $d_m(z)$ instead of $d_L(z)$ because we wanted our analysis to be purely data-dependent.

With the new dataset and a different method to test the goodness of fit, we could show the transition from deceleration to acceleration point with SN data alone, unlike the previous work; but the addition of GRB data increased the number of fitting functions that stay usable, and we got rid of couple of singularities that were present in the range $z = 0$ to 2.3, for SN data. Hence, we also added them. With their addition, we found the deceleration to acceleration transition to be at redshift $z_{t,\text{flat}} = 0.55^{+0.10}_{-0.07}$.

After the assumption of Einstein's General Relativity, we see that, as in previous work, there is a special redshift value at which the curvature of the universe has no effect on its energy density. With this point at hand, we managed to put an upper limit of approximately 0.47 ± 0.04 on the current density parameter of matter, only using luminosity distance data. With this parameter we also got a lower limit on current dark energy density parameter of $\Omega_{0,\text{de}} \gtrsim 0.32$; the minimum of the lower limits applies to the most negatively curved universe we considered, for other curvatures in the considered interval, the lower limit is higher. In particular, for the flat case $\Omega_{0,\text{de}} \gtrsim 0.50$.

We also used Starobinsky's gravity model, to see, if we can explain the data within the framework of the matter-dominated universe. We compare $\rho(z)$ that we got from the model to the matter-only curve (i.e $(\rho_{0\text{m,max}})(1+z)^3$) and tried to choose the α values (parameter of the model) that make the difference between them smallest.

We could not get anything useful from positive α values, but negative ones gave us good results, the best one being $\alpha = -10^{5.6}$ Mpc^2. So this model can explain the accelerated expansion of the universe without dark energy. However, the downside of using negative α's is that they give negative energy density at high redshift values. And, by dividing $\rho(0)$ (for flat case) by $\rho(0)$, from GR (critical density), we got a value for the current total density parameter as $\Omega_0 = 0.55$, meaning that in this model the amount of dark matter is more than two times that in the ΛCDM model.

REFERENCES

1. Hubble, E., "A Relation between Distance and Radial Velocity among Extra-Galactic Nebulae", *Proceedings of the National Academy of Science*, Vol. 15, pp. 168–173, Mar. 1929.

2. Weinberg, S., *Cosmology*, Oxford Univ. Press, 2008.

3. Çamlıbel, A. K., "On the history of expansion and matter-energy content of the universe", *PhD Thesis*, 2016.

4. Semiz, İ. and A. K. Çamlıbel, "What do the cosmological supernova data really tell us?", *Journal of Cosmology and Astroparticle Physics*, Vol. 2015, No. 12, p. 038, 2015.

5. Scolnic, D., D. Jones, A. Rest, Y. Pan, R. Chornock, R. Foley, M. Huber, R. Kessler, G. Narayan, A. Riess *et al.*, "The complete light-curve sample of spectroscopically confirmed SNe Ia from Pan-STARRS1 and cosmological constraints from the combined pantheon sample", *The Astrophysical Journal*, Vol. 859, No. 2, p. 101, 2018.

6. Suzuki, N., D. Rubin, C. Lidman, G. Aldering, R. Amanullah, K. Barbary, L. Barrientos, J. Botyanszki, M. Brodwin, N. Connolly *et al.*, "The Hubble Space Telescope Cluster Supernova Survey. V. Improving the dark-energy constraints above z>1 and building an early-type-hosted supernova sample", *The Astrophysical Journal*, Vol. 746, No. 1, p. 85, 2012.

7. Starobinsky, A. A., "A new type of isotropic cosmological models without singularity", *Physics Letters B*, Vol. 91, No. 1, pp. 99–102, 1980.

8. Utiyama, R. and B. S. DeWitt, "Renormalization of a classical gravitational field interacting with quantized matter fields", *Journal of Mathematical Physics*, Vol. 3,

No. 4, pp. 608–618, 1962.

9. Sotiriou, T. P. and V. Faraoni, "f (R) theories of gravity", *Reviews of Modern Physics*, Vol. 82, No. 1, p. 451, 2010.

10. Jaime, L. G., L. Patino and M. Salgado, "f (R) Cosmology revisited", *arXiv preprint arXiv:1206.1642*, 2012.

11. Riess, A. G., A. V. Filippenko, P. Challis, A. Clocchiatti, A. Diercks, P. M. Garnavich, R. L. Gilliland, C. J. Hogan, S. Jha, R. P. Kirshner *et al.*, "Observational evidence from supernovae for an accelerating universe and a cosmological constant", *The Astronomical Journal*, Vol. 116, No. 3, p. 1009, 1998.

12. Perlmutter, S., G. Aldering, G. Goldhaber, R. Knop, P. Nugent, P. Castro, S. Deustua, S. Fabbro, A. Goobar, D. Groom *et al.*, "Measurements of Ω and Λ from 42 high-redshift supernovae", *The Astrophysical Journal*, Vol. 517, No. 2, p. 565, 1999.

13. Caldwell, R. R., R. Dave and P. J. Steinhardt, "Cosmological imprint of an energy component with general equation of state", *Physical Review Letters*, Vol. 80, No. 8, p. 1582, 1998.

14. Caldwell, R. R., "A phantom menace? Cosmological consequences of a dark energy component with super-negative equation of state", *Physics Letters B*, Vol. 545, No. 1-2, pp. 23–29, 2002.

15. Carroll, S. M., V. Duvvuri, M. Trodden and M. S. Turner, "Is cosmic speed-up due to new gravitational physics?", *Physical Review D*, Vol. 70, No. 4, p. 043528, 2004.

16. Dvali, G., G. Gabadadze and M. Porrati, "4D gravity on a brane in 5D Minkowski space", *Physics Letters B*, Vol. 485, No. 1-3, pp. 208–214, 2000.

17. Richardson, D., R. L. Jenkins III, J. Wright and L. Maddox, "Absolute-magnitude distributions of supernovae", *The Astronomical Journal*, Vol. 147, No. 5, p. 118, 2014.

18. Perlmutter, S., S. Gabi, G. Goldhaber, A. Goobar, D. Groom, I. Hook, A. Kim, M. Kim, J. Lee, R. Pain *et al.*, "Measurements* of the Cosmological Parameters Ω and Λ from the First Seven Supernovae at z$\geq$ 0.35", *The astrophysical journal*, Vol. 483, No. 2, p. 565, 1997.

19. Schaefer, B. E., "The Hubble diagram to redshift>6 from 69 gamma-ray bursts", *The Astrophysical Journal*, Vol. 660, No. 1, p. 16, 2007.

20. Cattoën, C. and M. Visser, "Cosmography: Extracting the Hubble series from the supernova data", *arXiv preprint gr-qc/0703122*, 2007.

21. Aviles, A., C. Gruber, O. Luongo and H. Quevedo, "Cosmography and constraints on the equation of state of the Universe in various parametrizations", *Physical Review D*, Vol. 86, No. 12, p. 123516, 2012.

22. Abbott, B., R. Abbott, T. Abbott, M. Abernathy, F. Acernese, K. Ackley, C. Adams, T. Adams, P. Addesso, R. Adhikari *et al.*, "Observation of Gravitational Waves from a Binary Black Hole Merger", *Physical Review Letters*, Vol. 116, No. 6, p. 061102, 2016.

23. Gruber, C. and O. Luongo, "Cosmographic analysis of the equation of state of the universe through Padé approximations", *Physical Review D*, Vol. 89, No. 10, p. 103506, 2014.

24. Aviles, A., A. Bravetti, S. Capozziello and O. Luongo, "Precision cosmology with Padé rational approximations: Theoretical predictions versus observational limits", *Physical Review D*, Vol. 90, No. 4, p. 043531, 2014.

25. Wei, H., X.-P. Yan and Y.-N. Zhou, "Cosmological applications of Padé approxi-

mant", *Journal of Cosmology and Astroparticle Physics*, Vol. 2014, No. 01, p. 045, 2014.